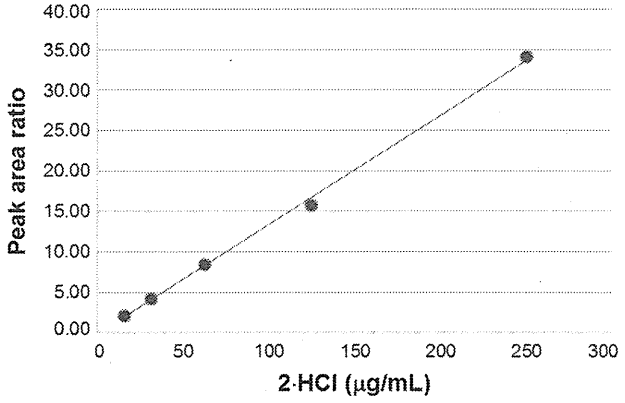

Figure 2. A calibration curve of compound **2·HCl** for calculating PK in rats.

2. Results and discussion

2.1. Calibration curve

Compound **2** was converted to its hydrochloride salt **2·HCl**, by treatment with 4 M HCl in dioxane. Standard solutions in saline of this HCl salt at concentrations over a range of 0–250 μg/mL were prepared and a calibration curve was constructed using the ratio of observed HPLC peak areas and concentrations of **2·HCl** to demonstrate the linearity shown in Figure 2.[14] The corresponding linear regression equation is $Y = 0.1345X$ ($R^2 = 0.9981$). Plasma concentrations of **2·HCl** were measured using this equation. The calibration curve shown in SD Figure S5C for the concentrations of compound **2** in plasma of a rhesus macaque was constructed using standard solutions of **2·HCl** in saline at concentrations over a range of 0–312.5 μg/mL. The linear regression equation in this case is $Y = 0.034X$ ($R^2 = 0.9927$). For adsorption of compound **2** by blood cells of a rhesus macaque, a calibration curve was constructed using standard solutions of **2·HCl** in saline at concentrations over a range of 0–950 μg/mL. The linear regression equation is $Y = 0.0553X$ ($R^2 = 0.9263$) and the curve is shown in SD Figure S7C.

2.2. Pharmacokinetics in rats

The primary stock solution of **2·HCl** was prepared in saline (2.5 mg/mL). Initially, the acute toxicity of compound **2** in rats was investigated to determine its maximum tolerated dose. The HCl salt, compound **2·HCl**, (0, 0.5, 1.0, 2.5 and 5.0 mg) was administered by tail vein injection into Jcl:SD rats (3 or 4 rats for each dose). Rats with the 5.0 mg administration showed a relatively low increase in the body weight although the intake amount of bait and water increased remarkably two weeks after administration, compared to the other rats (Supplementary data, SD Figs. S1 and S2). This observation suggested abnormalities such as renal and hepatic dysfunction and as a result, the maximum dose in rats of **2·HCl** was determined to be 2.5 mg.

Compound **2·HCl** (2.5 mg) in saline (1 mL) was administered at a level of 14 mg/kg by tail vein injection into Jcl:SD rats. Blood was collected from the tail vein into centrifugal blood collection tubes 15, 30, 45, 60, 120 and 240 min after administration of **2·HCl**. Plasma (50 μL) obtained from the blood sample was mixed with phenol in saline (final volume 60 μL) and centrifuged at 2000*g* for 3 min to remove any protein. The resultant supernatant was used in the analysis. A 50 μL aliquot of each filtrate was injected into HPLC by an autosampler. Compound **2** was detected in the HPLC analysis and was characterized by ESI-TOF-MS. The HPLC chart of the filtrate collected 30 min after administration of compound **2** is shown in Figure 3. Concentrations in blood of compound **2** after administration (15, 30, 45, 60, 120 and 240 min) were calculated using the calibration curve (SD Fig. S4) and plotted as shown in Figure 4.[15]

Using the data measured at 15, 30, 45, 60, 120 and 240 min, the half-life was calculated as 8.4 min by curve fitting with a one-compartment model based on GraphPad Prism Version 5.04 (GraphPad Software, CA, U.S.A). The initial concentration was calculated as 17.3 μg/mL. Compound **2** has a low molecular weight (317.4) and some level of hydrophobicity based on its structure, suggesting that the renal excretion is unlikely. At a dose of 2500 (μg)/initial concentration 17.3 (μg/mL), the volume of distribution was calculated as 145 mL, suggesting widespread tissue distribution of **2** as a result of its hydrophobicity.

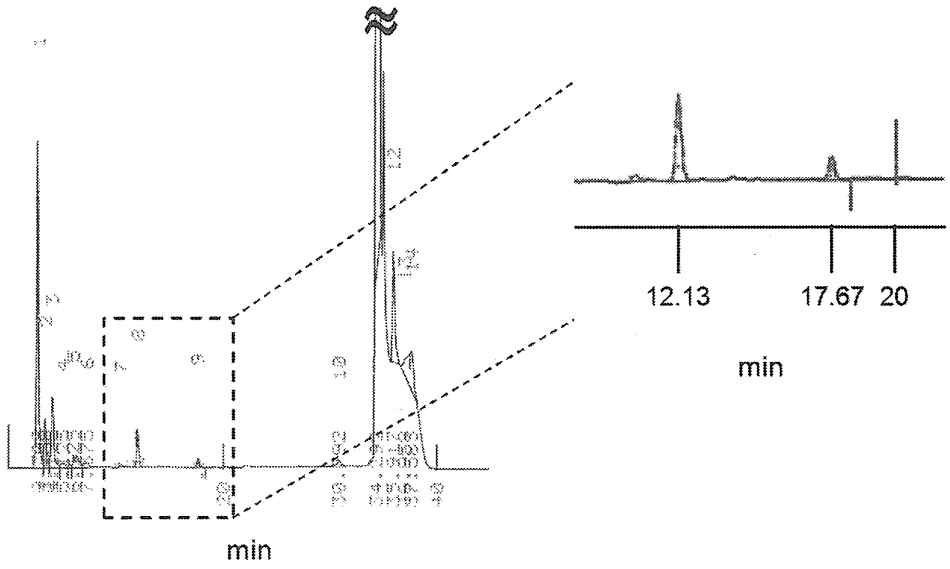

Figure 3. HPLC chart of rat plasma 30 min after intravenous administration of compound **2**. The plasma sample was eluted with a linear gradient of 20–35% CH_3CN (0.1% TFA, in 30 min). Peak 8 (retention time: 12.13 min) corresponds to the internal standard (phenol) and peak 9 (retention time: 17.67 min) corresponds to compound **2**.

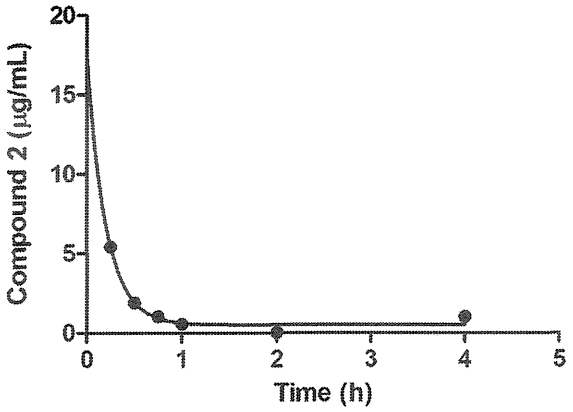

Figure 4. Plots of concentrations in rat blood of compound **2** after administration (15, 30, 45, 60, 120 and 240 min). Half-life is calculated as 0.141 h (8.4 min). The plasma of a representative rat was used for the analyses.

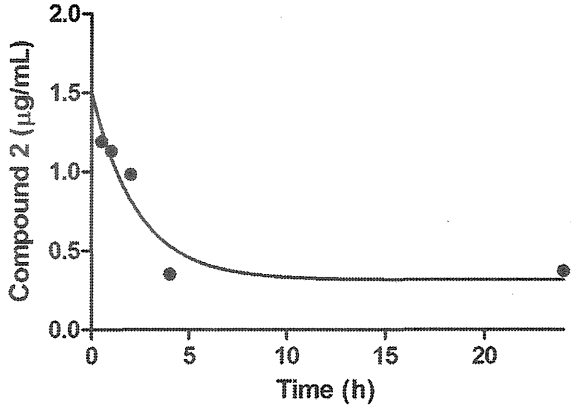

Figure 6. Plots of macaque blood concentrations of compound **2** after administration of **2**·**HCl** (0.5, 1, 2, 4 and 24 h). Half-life is calculated as 1.64 h (98.4 min). The plasma of a rhesus macaque was used for the analyses.

2.3. Pharmacokinetics in a rhesus macaque

The primary stock solution of the **2**·**HCl** was prepared in potassium-free phosphate-buffered saline (Na_2HPO_4 + NaH_2PO_4 + NaCl, pH 7.4) (2.4 mg/mL) to avoid hyperpotassemia and acidosis. Initially, the acute toxicity observed by treatment with **2**·**HCl** in a rhesus macaque was investigated to determine the maximum tolerated dose. **2**·**HCl** (14.1, 35.3 and 70.6 mg) was administered by cephalic vein injection into a rhesus macaque (one macaque for each dose). A macaque administered 70.6 mg, showed abnormalities such as mydriasis, prolonged PR interval in the electrocardiogram and bradycardia, while acute toxicity was not observed following the administration of **2**·**HCl** at levels up to 35.3 mg[16] and the maximum tolerated dose in a rhesus macaque was determined to be 35.3 mg (6.7 mg/kg). The macaque which had been administered 70.6 mg of **2**·**HCl** was treated by an emergency intervention with dobutamine (iv).

Compound **2**·**HCl** (70.6 mg) was intravenously administered at 13.4 mg/kg into a rhesus macaque. Blood (3.0 mL) was collected from cephalic vein 0, 0.5, 1, 2, 4 and 24 h after administration of the hydrochloride using winged needles. Plasma (60 μL) obtained from the blood sample was mixed with MeOH (200 μL) to remove plasma proteins and then centrifuged at 2000*g* for 3 min at room temperature in a microcentrifuge (MCF-2360, LMS Co., Ltd., Tokyo, Japan). A 228 μL aliquot of each supernatant was mixed with 12 μL of phenol in saline (stock solution: 0.3 mg/mL) to give a final concentration of phenol of 150 μg/mL, then filtered. A 200 μL aliquot of each filtrate was analyzed by HPLC using phenol as an internal standard. Compound **2** was detected in the HPLC analysis of each filtrate and its peak was characterized by ESI-TOF-MS. The HPLC of the filtrate prepared 30 min after administration of **2**·**HCl** is shown in Figure 5. Blood concentrations of compound **2** after 0.5, 1, 2, 4 or 24 h administration were calculated using the calibration curve (SD Fig. S6) and plotted as shown in Figure 6.

Using the time-course data, the half-life was calculated as 98.4 min by curve fitting based on GraphPad Prism Version 5.04 (GraphPad Software, CA, U.S.A.). The initial concentration in blood was also calculated as 1.50 μg/mL. In a macaque, this suggests that the renal excretion is not possible and this was by the absence of compound **2** in the HPLC analysis of the urine (SD). The distribution volume was calculated as 47.1 L; the dose 70.6 (mg)/initial concentration 1.50 (μg/mL) ratio suggests tissue distribution.

2.4. Adsorption of compound 2 to blood cells of a rhesus macaque

The question of whether compound **2** can be attached to and adsorbed into blood cells was investigated. Initially, **2**·**HCl** was added to blood (1 mL) of a rhesus macaque reaching a final concentration of 1 mg/mL. This mixture was incubated at 37 °C for 0, 1 and 2 h, and then centrifuged at 3600 rpm for 5 min at room temperature in a microcentrifuge to separate plasma (730 μL) from

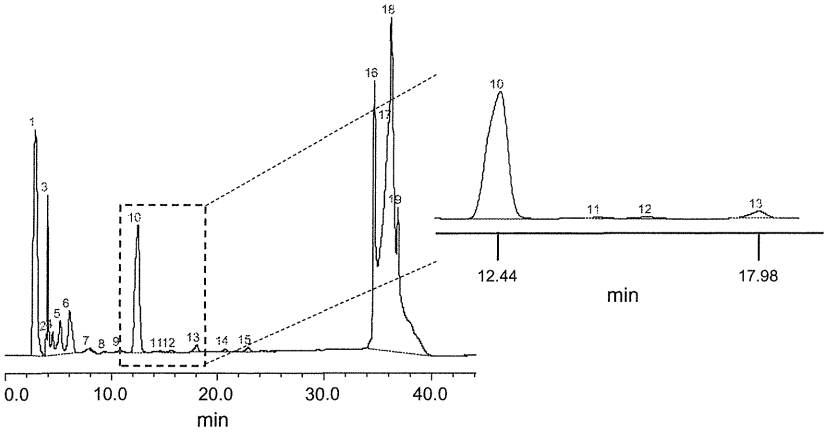

Figure 5. HPLC chart of macaque plasma 30 min after intravenous administration of **2**·**HCl**. The plasma sample was eluted with a linear gradient of 20–35% CH_3CN (0.1% TFA, in 30 min). Peak 10 (retention time: 12.44 min) corresponds to the internal standard (phenol) and peak 13 (retention time: 17.98 min) corresponds to compound **2**.

blood cells. In addition, plasma (0.5 mL) was added to the blood cells incubated for 1 h, then the mixture was incubated again for 1 h to separate plasma (730 μL) from the blood cells. Blood cell samples were prepared by mixing the blood cells with 480 μL of PBS and diluting the mixture to 1 mL with PBS. Blood cell samples were sonicated to disrupt cell membranes then both plasma and blood cell samples (60 μL each) were vortex-mixed with 200 μL of MeOH, then centrifuged at 2000g for 3 min at room temperature. A 228 μL aliquot of each supernatant was mixed with 12 μL of phenol in saline (final concentration: 600 μg/mL) and filtered. A 200 μL aliquot of each filtrate was injected to HPLC by an autosampler (SD Fig. S8).

The fractions of plasma and blood cells were analyzed by HPLC to quantify compound **2** (Fig. 7). The results showed that incubation enhanced the attachment or adsorption of compound **2** to blood cells; incubation for 1 or 2 h led to percentages of 39.7% and 39.3%, respectively, in distribution in cells, prior to incubation there was a distribution percentage of 34.8% in cells. Furthermore, compound **2**, which was adsorbed into blood cells, was significantly redistributed in plasma when fresh plasma was added; the addition of plasma to blood cells incubated for 1 h and a further incubation for 1 h caused redistribution of compound **2** to plasma and a reduction of distribution percentages to cells from 39.7% to 11.5%. This suggests that compound **2**, which was attached to blood cells, might be transferred from the cells to plasma and subsequently distributed to tissues.

These results indicate that the concentration in blood of compound **2** might be reduced, ultimately to ~1 mg/mL (3 μM) with 2–4 h treatments in rats (14 mg/kg) and rhesus macaques (13.4 mg/kg). The EC_{50} value of compound **2** has been determined as 10–50 μM in laboratory and primary HIV-1 strains.[11] Thus, in several hours after intravenous administration of compound **2** the efficacy might be diminished because the concentration in blood of compound **2** is being maintained below EC_{50} levels. However, the amount administered cannot be increased because of the acute toxicity which is described in the previous section, although the concentration in blood of compound **2** does not reach its CC_{50} level of 210 μM.[11] Recently, we reported that CD4 mimics such as compound **1** enhance the binding potency of anti-gp120 monoclonal antibodies such as KD-247[16] toward an envelope protein gp120, showing synergistic neutralization.[13] Compound **2** also enhances the neutralizing activity of KD-247 against simian–human immunodeficiency virus (SHIV)-KS661 strain via highly synergistic interactions. When compound **2** is used in combination with anti-gp120 monoclonal antibodies such as KD-247, the level of compound **2** of 3 μM might be sufficient for neutralization in vivo and thus it might be possible to reduce the dose of compound **2**. In addition, we also found that compound **1** and CXCR4 antagonists such as T140[2] showed synergistic anti-HIV-1 activity,[11] Thus, a combinatorial use with co-receptor antagonists would be also effective for reduction of the dose of compound **2**.

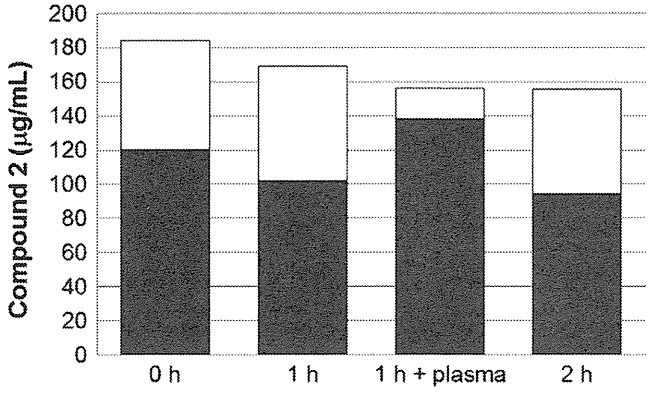

Figure 7. Quantitative analysis of compound **2** contained in macaque blood cells and plasma after incubation for 0, 1, or 2 h. 1 h + plasma means the addition of plasma (0.5 mL) to 1 h incubated blood cells followed by further incubation for 1 h. Concentrations of compound **2** in plasma are shown in black bars, and those in blood cells are shown in white bars.

3. Conclusion

CD4 mimics are attractive not only as HIV entry inhibitors but also possibly as cooperating agents for neutralizing antibodies. Binding of CD4 mimicking compounds to gp120 causes a conformational change in gp120. In this way, CD4 mimics function as 'envelope openers' and enhance the binding ability of anti-gp120 neutralizing antibodies. We discovered lead compound **2** with relatively high potency and low cytotoxicity in our previous study. In the current study, the pharmacokinetics of compound **2** in rats and rhesus macaques in the intravenous administration were investigated. Plots of plasma concentrations of compound **2** fitted with a one-compartment model provided calculation of half-lives of compound **2** in blood in rats and rhesus macaques: 8.4 and 98.4 min, respectively, suggesting that compound **2** is broadly distributed in tissues. A few hours post-injection, plasma concentrations of compound **2** in both species stabilized at micromolar levels. Consequently, compound **2** might have promise as a lead compound for the intravenous administration in a cocktail therapy with anti-gp120 monoclonal antibodies such as KD-247 and with co-receptor antagonists such as T140.[2]

4. Experimental

4.1. General information

A Cosmosil 5C18-ARII column (4.6 × 250 mm, Nacalai Tesque, Inc., Kyoto, Japan) was used for analytical HPLC, with a linear gradient of CH_3CN containing 0.1% (v/v) TFA at a flow rate of 1 cm^3 min^{-1} on a JASCO PU-2089 plus (JASCO Corporation, Ltd., Tokyo, Japan), and eluents were detected by UV at 220 nm on a JASCO UV-2075 plus (JASCO Corporation, Ltd, Tokyo, Japan). Samples were injected by an autosampler on a JASCO AS-2075 plus (JASCO Corporation, Ltd, Tokyo, Japan). ESI-TOF-MS were recorded on a micrOTOF-2focus (Bruker Daltonics) mass spectrometer.

4.2. Calibration curve

To compound **2** (1.0 g) in MeOH (5 mL) was added 4 M HCl/dioxane (10 mL) and the mixture was stirred for 30 min at room temperature. The mixture was concentrated under reduced pressure and the **2**·**HCl** was precipitated in cooled Et_2O (yield: 1.2 g, quantitative).

To construct a pharmacokinetics calibration curve in a rat, standard stock solutions in saline of **2**·**HCl**; 263, 131.5, 65.8, 32.9 and 16.4 μg/mL and an internal standard stock solution; 1.25 mg/mL phenol in saline were prepared. Each standard stock solution (22.8 μL) was mixed with 1.2 μL of the internal stock solution to give a total volume of 24 μL, then filtered. A 20 μL aliquot of each filtrate was injected to HPLC. The final concentration of **2**·**HCl** was 250, 125, 62.5, 31.3 or 15.6 μg/mL and each sample contains 62.5 μg/mL phenol. Elution was carried out with a linear gradient of 20–35% CH_3CN (0.1% TFA) over 30 min (SD Fig. S3). A calibration curve was constructed using the ratio of HPLC peak areas and concentrations of **2**·**HCl** to demonstrate the linearity as shown in Figure 2. The linear regression equation is $Y = 0.1345X$ ($R^2 = 0.9981$).

To construct a pharmacokinetics calibration curve in a rhesus macaque, standard stock solutions in saline of **2**·**HCl** (329, 164.5,

82.3, 41.1, 20.6 and 10.3 μg/mL) and an internal standard stock solution of phenol in saline (3 mg/mL) were prepared. Each standard stock solution (22.8 μL) was mixed with 1.2 μL of the internal stock solution and filtered. A 20 μL aliquot of each filtrate was injected to HPLC. The final concentration of **2·HCl** was 312.5, 156.3, 78.1, 39.1, 19.5 and 9.77 μg/mL, each contained 150 μg/mL phenol. Elution was carried out with a linear gradient of 20–35% CH_3CN (0.1% TFA) over 30 min. A calibration curve was constructed using the ratio of HPLC peak areas and concentrations of **2·HCl** to demonstrate the linearity as shown in SD Figure S5. The linear regression equation is $Y = 0.034X$ ($R^2 = 0.9927$).

To construct a calibration curve for the adsorption experiments, standard stock solutions in saline of **2·HCl**; 1000, 500, 250, 100, 50 μg/mL and an internal standard stock solution of 12 mg/mL phenol in saline were prepared. Each standard stock solution (228 μL) was mixed with 12 μL of the internal stock solution and filtered. A 200 μL aliquot of each filtrate was injected to HPLC by an autosampler. The final concentration of **2·HCl** was 950, 475, 238, 95.0 and 47.5 μg/mL and contained 600 μg/mL phenol. Elution was carried out with a linear gradient of 20–35% CH_3CN (0.1% TFA) over 30 min. A calibration curve was constructed using the ratio of HPLC peak areas and concentrations of **2·HCl** to demonstrate the linearity shown in SD Figure S7. The linear regression equation is $Y = 0.0553X$ ($R^2 = 0.9263$).

4.3. Pharmacokinetics in rats

Experiments using rats were conducted in an animal facility under specific pathogen-free conditions, in compliance with institutional regulations approved by the Committee of Tokyo Medical and Dental University (Tokyo, Japan). Five-week-old Jcl:SD rats purchased from CLEA Japan, Inc. (Tokyo, Japan) were maintained for one week before experiments. Compound **2·HCl** (2.5 mg) in 1.0 mL of saline was administered by tail vein injection into 6 week-old Jcl:SD rats. Blood was collected from the tail vein into centrifugal blood collection tubes (E·DS11, Eiken Chemical Co., Ltd., Tokyo, Japan) 15, 30, 45, 60, 120 and 240 min after administration. Blood was centrifuged at 2000*g* for 3 min at room temperature to separate plasma and stored at −80 °C before use. A freeze-thawed plasma sample (50 μL) was mixed with 10 μL of phenol in saline (stock solution: 0.375 mg/mL, giving a final concentration of 62.5 μg/mL) and filtered at 2000*g* for 3 min in a microcentrifuge (MCF-2360, LMS Co., Ltd., Tokyo, Japan). A 50 μL aliquot of each filtrate was injected into an HPLC. Elution was carried out with a linear gradient of 20–35% CH_3CN (0.1% TFA) over 30 min shown in SD Figure S4. Compound **2** was detected in the HPLC analysis and its peak was characterized by ESI-TOF-MS (*m/z* calcd for $C_{18}H_{28}N_3O_2$ $[M+H]^+$ 318.22, found 318.19).

4.4. Pharmacokinetics in a rhesus macaque

Experiments using an adult female rhesus macaque, seven years old, were conducted in a biosafety level 3 animal facility, in compliance with institutional regulations approved by the Committee for Experimental Use of Nonhuman Primates of the Institute for Virus Research, Kyoto University (Kyoto, Japan). Compound **2·HCl** (70.6 mg) in 30 mL of 0.1 M sodium phosphate buffer containing NaCl (pH 7.4) was administered by cephalic vein injection. Blood (3.0 mL) was collected from the cephalic vein 0, 0.5, 1, 2, 4 and 24 h after administration using winged needles. Blood was centrifuged at 3600 rpm for 5 min at room temperature to separate plasma then stored at −80 °C before use. A freeze-thawed plasma sample (60 μL) was vortex-mixed with MeOH (200 μL) and centrifuged at 2000*g* for 3 min at room temperature. A 228 μL aliquot of each supernatant was mixed with 12 μL of phenol in saline (stock solution: 0.3 mg/mL, final concentration: 150 μg/mL) and filtered. A 200 μL aliquot of each filtrate was injected into HPLC by an autosampler. Elution was carried out with a linear gradient of 20–35% CH_3CN (0.1% TFA) over 30 min shown in SD Figure S6. Compound **2** was detected in the HPLC analysis of each filtrate and its peak was characterized by ESI-TOF-MS (*m/z* calcd for $C_{18}H_{28}N_3O_2$ $[M+H]^+$ 318.22, found 318.19).

4.5. Adsorption experiments of compound 2 to blood cells of a rhesus macaque

Compound **2·HCl** in saline (5 mg/mL, 0.25 mL) was added to blood (1.0 mL) collected from a macaque, and incubated at 37 °C for 0, 1 and 2 h. After incubation, plasma samples (730 μL) were separated by centrifugation at 3600 rpm for 5 min at room temperature, and PBS (480 μL) was added to the resulting precipitates, increasing their total volume to 1.0 mL, and producing blood cell samples. In addition, plasma (0.5 mL) was added to the blood cells after 1 h incubation and the mixture was incubated again for 1 h to separate plasma (730 μL) and blood cells. The separated plasma and blood cell samples were stored at −80 °C before use. Freeze-thawed plasma samples (60 μL) were vortex-mixed with MeOH (200 μL) and centrifuged at 2000*g* for 3 min at room temperature. Freeze-thawed blood cell samples (200 μL) were sonicated to disrupt cell membranes (Sonifier 250, Branson Ultrasonics, Emerson Japan Ltd., Kanagawa, Japan), and 60 μL of the sonicated products was vortex-mixed with MeOH (200 μL) and centrifuged at 2000*g* for 3 min at room temperature. A 228 μL aliquot of each supernatant obtained from both plasma and blood cell samples was mixed with 12 μL of phenol in saline (stock solution: 12 mg/mL, final concentration: 600 μg/mL) and filtered. After filtration, a 200 μL aliquot of each filtrate was injected into HPLC by an autosampler. Elution was carried out with a linear gradient of 20–35% CH_3CN (0.1% TFA) over 30 min and is shown in SD Figure S8.

Acknowledgments

This work was supported in part by Grant-in-Aid for Scientific Research from the Ministry of Education, Culture, Sports, Science, and Technology of Japan, and Health and Labour Sciences Research Grants from Japanese Ministry of Health, Labor, and Welfare. The authors thank Ms. Misako Namae and Professor Hiroshi Nishina, Medical Research Institute, Tokyo Medical and Dental University, for providing us with methods for the collection of blood from rats. The authors also thank Dr. Fumiyoshi Yamashita, Graduate School of Pharmaceutical Sciences, Kyoto University, for assistance with the calculation of the pharmacokinetics. Our thanks are also extended to Ms. Yuko Yamada and Ms. Aki Ohya, from our laboratory, for teaching us techniques for analysis of plasma samples.

Supplementary data

Supplementary data (figures of changes on body weight and on intake amounts of bait and water in rats, tables of HPLC peak areas and HPLC charts) associated with this article can be found, in the online version, at http://dx.doi.org/10.1016/j.bmc.2013.10.005.

References and notes

1. Hashimoto, C.; Tanaka, T.; Narumi, T.; Nomura, W.; Tamamura, H. *Expert Opin. Drug Discovery* **2011**, *6*, 1067.
2. (a) Tamamura, H.; Xu, Y.; Hattori, T.; Zhang, X.; Arakaki, R.; Kanbara, K.; Omagari, A.; Otaka, A.; Ibuka, T.; Yamamoto, N.; Nakashima, H.; Fujii, N. *Biochem. Biophys. Res. Commun.* **1998**, *253*, 877; (b) Tamamura, H.; Omagari, A.; Oishi, S.; Kanamoto, T.; Yamamoto, N.; Peiper, S. C.; Nakashima, H.; Otaka, A.; Fujii, N. *Bioorg. Med. Chem. Lett.* **2000**, *10*, 2633; (c) Fujii, N.; Oishi, S.; Hiramatsu, K.; Araki, T.; Ueda, S.; Tamamura, H.; Otaka, A.; Kusano, S.; Terakubo, S.; Nakashima, H.; Broach, J. A.; Trent, J. O.; Wang, Z.; Peiper, S. C. *Angew. Chem., Int. Ed.* **2003**, *42*, 3251; (d) Tamamura, H.; Hiramatsu, K.; Ueda,

S.; Wang, Z.; Kusano, S.; Terakubo, S.; Trent, J. O.; Peiper, S. C.; Yamamoto, N.; Nakashima, H.; Otaka, A.; Fujii, N. *J. Med. Chem.* **2005**, *48*, 380; (e) Tamamura, H.; Araki, T.; Ueda, S.; Wang, Z.; Oishi, S.; Esaka, A.; Trent, J. O.; Nakashima, H.; Yamamoto, N.; Peiper, S. C.; Otaka, A.; Fujii, N. *J. Med. Chem.* **2005**, *48*, 3280.

3. Chan, D. C.; Kim, P. S. *Cell* **1998**, *93*, 681.
4. Eckert, D. M.; Kim, P. S. *Annu. Rev. Biochem.* **2001**, *70*, 777.
5. Wyatt, R.; Sodroski, J. *Science* **1884**, *1998*, 280.
6. Berger, E. A.; Murphy, P. M.; Farber, J. M. *Annu. Rev. Immunol.* **1999**, *17*, 657.
7. (a) Wild, C. T.; Shugars, D. C.; Greenwell, T. K.; McDanal, C. B.; Matthews, T. J.; Chan, D. C.; Fass, D. *Proc. Natl. Acad. Sci. U.S.A.* **1994**, *91*, 9770; (b) Berger, J. M.; Kim, P. S. *Cell* **1997**, *89*, 263; (c) Otaka, A.; Nakamura, M.; Nameki, D.; Kodama, E.; Uchiyama, S.; Nakamura, S.; Nakano, H.; Tamamura, H.; Kobayashi, Y.; Matsuoka, M.; Fujii, N. *Angew. Chem., Int. Ed.* **2002**, *41*, 2937; (d) Nomura, W.; Hashimoto, C.; Ohya, A.; Miyauchi, K.; Urano, E.; Tanaka, T.; Narumi, T.; Nakahara, T.; Komano, J. A.; Yamamoto, N.; Tamamura, H. *ChemMedChem* **2012**, *7*, 205; (e) Hashimoto, C.; Nomura, W.; Ohya, A.; Urano, E.; Miyauchi, K.; Narumi, T.; Aikawa, H.; Komano, J. A.; Yamamoto, N.; Tamamura, H. *Bioorg. Med. Chem.* **2012**, *20*, 3287; (f) Nomura, W.; Hashimoto, C.; Suzuki, T.; Ohashi, N.; Fujino, M.; Murakami, T.; Yamamoto, N.; Tamamura, H. *Bioorg. Med. Chem.* **2013**, *21*, 4452.
8. Zhao, Q.; Ma, L.; Jiang, S.; Lu, H.; Liu, S.; He, Y.; Strick, N.; Neamati, N.; Debnath, A. K. *Virology* **2005**, *339*, 213.
9. (a) Madani, N.; Schön, A.; Princiotto, A. M.; LaLonde, J. M.; Courter, J. R.; Soeta, T.; Ng, D.; Wang, L.; Brower, E. T.; Xiang, S.-H.; Do Kwon, Y.; Huang, C.-C.; Wyatt, R.; Kwong, P. D.; Freire, E.; Smith, A. B., 3rd; Sodroski, J. *Structure* **2008**, *16*, 1689; (b) LaLonde, J. M.; Elban, M. A.; Courter, J. R.; Sugawara, A.; Soeta, T.; Madani, N.; Princiotto, A. M.; Kwon, Y. D.; Kwong, P. D.; Schön, A.; Freire, E.; Sodroski, J.; Smith, A. B., 3rd *Bioorg. Med. Chem. Lett.* **2011**, *20*, 354; (c) LaLonde, J. M.; Kwon, Y. D.; Jones, D. M.; Sun, A. W.; Courter, J. R.; Soeta, T.; Kobayashi, T.; Princiotto, A. M.; Wu, X.; Schön, A.; Freire, E.; Kwong, P. D.; Mascola, J. R.; Sodroski, J.; Madani, N.; Smith, A. B., 3rd *J. Med. Chem.* **2012**, *55*, 4382.
10. Curreli, F.; Choudhury, S.; Pyatkin, I.; Zagorodnikov, V. P.; Bulay, A. K.; Altieri, A.; Kwon, Y. D.; Kwon, P. D.; Debnath, A. K. *J. Med. Chem.* **2012**, *55*, 4764.
11. (a) Yamada, Y.; Ochiai, C.; Yoshimura, K.; Tanaka, T.; Ohashi, N.; Narumi, T.; Nomura, W.; Harada, S.; Matsushita, S.; Tamamura, H. *Bioorg. Med. Chem. Lett.* **2010**, *20*, 354; (b) Narumi, T.; Ochiai, C.; Yoshimura, K.; Harada, S.; Tanaka, T.; Nomura, W.; Arai, H.; Ozaki, T.; Ohashi, N.; Matsushita, S.; Tamamura, H. *Bioorg. Med. Chem. Lett.* **2010**, *20*, 5853; (c) Narumi, T.; Arai, H.; Yoshimura, K.; Harada, S.; Nomura, W.; Matsushita, S.; Tamamura, H. *Bioorg. Med. Chem.* **2011**, *19*, 6735; (d) Narumi, T.; Arai, H.; Yoshimura, K.; Harada, S.; Hirota, Y.; Ohashi, N.; Hashimoto, C.; Nomura, W.; Matsushita, S.; Tamamura, H. *Bioorg. Med. Chem.* **2013**, *21*, 2518.
12. Schön, A.; Madani, N.; Klein, J. C.; Hubicki, A.; Ng, D.; Yang, X.; Smith, A. B., 3rd; Sodroski, J.; Freire, E. *Biochemistry* **2006**, *45*, 10973; (b) Schön, A.; Lam, S. Y.; Freire, E. *Future Med. Chem.* **2011**, *3*, 1129.
13. Yoshimura, K.; Harada, S.; Shibata, J.; Hatada, M.; Yamada, Y.; Ochiai, C.; Tamamura, H.; Matsushita, S. *J. Virol.* **2010**, *84*, 7558.
14. Mao, S.; Jin, H.; Bi, Y.-Q.; Liang, Z.; Li, H.; Hou, S.-X. *Chem. Pharm. Bull.* **2007**, *55*, 753.
15. Sakai-Kato, K.; Nanjo, K.; Kawanishi, T.; Okuda, H. *Chem. Pharm. Bull.* **2012**, *60*, 391.
16. Eda, Y.; Takizawa, M.; Murakami, T.; Maeda, H.; Kimachi, K.; Yonemura, H.; Koyanagi, S.; Shiosaki, K.; Higuchi, H.; Makizumi, K.; Nakashima, T.; Osatomi, K.; Tokiyoshi, S.; Matsushita, S.; Yamamoto, N.; Honda, M. *J. Virol.* **2006**, *80*, 5552.

Journal of General Virology (2013), **94**, 2710–2716 **DOI** 10.1099/vir.0.055590-0

Short Communication

Generation of a replication-competent simian–human immunodeficiency virus, the neutralization sensitivity of which can be enhanced in the presence of a small-molecule CD4 mimic

Hiroyuki Otsuki,[1] Takayuki Hishiki,[1] Tomoyuki Miura,[1] Chie Hashimoto,[2] Tetsuo Narumi,[2] Hirokazu Tamamura,[2] Kazuhisa Yoshimura,[3] Shuzo Matsushita[4] and Tatsuhiko Igarashi[1]

Correspondence
Tatsuhiko Igarashi
tigarash@virus.kyoto-u.ac.jp

[1]Laboratory of Primate Model, Experimental Research Center for Infectious Diseases, Institute for Virus Research, Kyoto University, Kyoto 606-8507, Japan

[2]Department of Medicinal Chemistry, Institute of Biomaterials and Bioengineering, Tokyo Medical and Dental University, Tokyo 101-0062, Japan

[3]AIDS Research Center, National Institute of Infectious Diseases, Tokyo 162-8640, Japan

[4]Division of Clinical Retrovirology and Infectious Diseases, Center for AIDS Research, Kumamoto University, Kumamoto 860-0811, Japan

Received 29 May 2013
Accepted 10 September 2013

Simian–human immunodeficiency virus (SHIV) carrying the envelope from the clade B clinical human immunodeficiency virus type 1 (HIV-1) isolate MNA, designated SHIV MNA, was generated through intracellular homologous recombination. SHIV MNA inherited biological properties from the parental HIV-1, including CCR5 co-receptor preference, resistance to neutralization by the anti-V3 loop mAb KD-247 and loss of resistance in the presence of the CD4-mimic small-molecule YYA-021. SHIV MNA showed productive replication in rhesus macaque PBMCs. Experimental infection of a rhesus macaque with SHIV MNA caused a transient but high titre of plasma viral RNA and a moderate antibody response. Immunoglobulin in the plasma at 24 weeks post-infection was capable of neutralizing SHIV MNA in the presence but not in the absence of YYA-021. SHIV MNA could serve a model for development of novel therapeutic interventions based on CD4-mimic-mediated conversion of envelope protein susceptible to antibody neutralization.

Control of primate lentiviral infection by antibodies directed against viral envelope protein is theoretically feasible. This was confirmed by the successful protection of macaque monkeys from challenge inoculation with simian–human immunodeficiency virus (SHIV) carrying an envelope protein (Env). Env was derived from a laboratory strain of human immunodeficiency virus type 1 (HIV-1) through the passive immunization of neutralizing mAbs directed against HIV-1 (Mascola *et al.*, 2000; Nishimura *et al.*, 2003). This neutralization is consistent with the results normally seen in cell culture systems.

In contrast, clinical isolates of HIV-1 that have not been subjected to extensive passage in T-cell lines are generally resistant to antibody-mediated neutralization (Moore *et al.*, 1995). It has been shown that virus in infected individuals is under selective pressure to develop a variety of means to evade attack by neutralizing antibodies, including sequence variation, glycosylation, tertiary structural shielding formed by the Env trimer and the rapid kinetics of conformational changes of Env, which affect fusion between the viral envelope and the plasma membrane of target cells (Kong & Sattentau, 2012). Although four major neutralizing epitopes have been identified in HIV-1 Env (i.e. the V1/V2 loop, the glycan-V3 site and CD4-binding site of gp120, and the membrane-proximal external region of gp41), for reasons that are as yet unclear few reports of antibodies directed against these epitopes capable of neutralizing a broad range of isolates have been published (Kwong & Mascola, 2012). High titres of antibodies directed against the V3 loop are elicited in individuals during the early phase of HIV-1 infection, but these are incapable of neutralizing the virus because the epitope in functional Env trimer is probably shielded from the antibody (Davis *et al.*, 2009b). Therefore, it is necessary to develop a means of rendering these epitopes accessible to

One supplementary table and five supplementary figures are available with the online version of this paper.

the antibodies, to make antibody-mediated suppression of HIV-1 a valid therapeutic option.

It has been reported that neutralization mediated by antibodies directed against the V3 loop (Lusso *et al.*, 2005) or CD4-induced epitope (CD4i) (Thali *et al.*, 1993) can be enhanced in the presence of soluble CD4 (sCD4). It is known that the interaction of Env with sCD4 drives a conformational change of the viral protein and makes the cryptic/occult epitopes accessible to these antibodies (Wyatt *et al.*, 1998). Small molecules that emulate sCD4 for its interaction and subsequent induction of conformational change of Env may be employed to intensify antibody-mediated interventions against HIV-1 infection. Compounds with the above-mentioned properties (i.e. NBD-556 and NBD-557) have been reported previously (Zhao *et al.*, 2005). NBD-556 has been shown in cell culture to interact with the CD4-binding pocket to induce a conformational change in gp120 (Madani *et al.*, 2008) and enhance exposure of the Env of primary HIV-1 isolates to neutralizing epitopes (Yoshimura *et al.*, 2010).

The present study was performed to evaluate small-molecule CD4-mimic-based enhancement of antibody-mediated virus neutralization, in the context of virus infection *in vivo*. The SHIV/macaque monkey model of AIDS is particularly suitable for such studies, as SHIV carries the HIV-1 Env and the neutralization sensitivity of SHIV is comparable to that of the parental HIV-1 (Shibata & Adachi, 1992).

As NBD-556, unlike sCD4, inhibits infection with select HIV-1 isolates (Yoshimura *et al.*, 2010), we generated a new SHIV strain carrying Env, the sensitivity of which to antibody-mediated neutralization is enhanced in the presence of a CD4 mimic. An HIV-1 isolate (MNA), previously designated primary isolate HIV-1 Pt.3, was used as the source of Env, as the viral protein has been reported to interact with NBD-556 (Yoshimura *et al.*, 2010). While the virus belongs to a distinct subset of HIV-1 isolates, as mentioned above, it has also been reported to utilize the CCR5 molecule to gain entry into target cells, a property that is shared by the majority of HIV-1 strains (Yoshimura *et al.*, 2010). A mAb directed against the tip of the V3 loop (GPGR motif), KD-247 (Eda *et al.*, 2006), was employed to assess this concept, as HIV-1 MNA is resistant to KD-247-mediated neutralization, despite carrying the exact epitope sequence in the tip of the V3 loop, and is converted to being sensitive to the antibody by NBD-556 in a dose-dependent manner (Yoshimura *et al.*, 2010).

First, we reproduced the results of Yoshimura *et al.* (2010) using a neutralization assay employing TZM-bl cells (Platt *et al.*, 1998), obtained from the National Institutes of Health (NIH) AIDS Reagent Program (Fig. S1, available in JGV Online). The virus was resistant to KD-247, as described previously, and required almost 50 μg ml^{-1} of the antibody to achieve 50 % neutralization in our assay. However, the observed resistance was eliminated in the presence of 2 μM NBD-556; 50 % neutralization was achieved in the presence of ~0.1 μg KD-247 ml^{-1}, corresponding to 1/500 of the amount of the antibody to achieve the same degree of neutralization in the absence of the CD4 mimic.

With reproduction of the properties of HIV-1 MNA Env, we generated an SHIV strain carrying Env through intracellular homologous recombination, as described previously (Fujita *et al.*, 2013) with minor modifications (Fig. S2). DNA fragments representing the 5′ and 3′ ends of the SHIV genome (fragments I and II, respectively) were amplified by PCR from the proviral DNA plasmid SHIV KS661. A DNA fragment containing *env* (fragment III) was amplified from cDNA of the HIV-1 MNA genome, which was prepared from virus particles (virion-associated RNA) in the culture supernatant of PM1/CCR5 cells (Yusa *et al.*, 2005) infected with the virus. The PCR primers used are listed in Table S1. Using a FuGENE HD transfection reagent, lipofection was performed on the C8166-CCR5 cells (Shimizu *et al.*, 2006) to co-transfect them with 0.2 μg DNA. A cytopathic effect, presumably caused by the emerged recombinant virus, was observed on day 13 post-transfection. The emerged virus, designated SHIV MNA, carried the entire gp120 and three-quarters of gp41 from HIV-1 MNA Env (Fig. 1a). The rest of Env was from SHIV KS661, the Env of which was derived from HIV-1 89.6 (Shinohara *et al.*, 1999). The CD4 binding site, and the regions and elements that reportedly interact with NBD-556 (Madani *et al.*, 2008; Yoshimura *et al.*, 2010), are preserved in SHIV MNA Env (Fig. S3). The virus was replication competent in PM1/CCR5 cells (data not shown).

As HIV-1 MNA has been suggested to be a CCR5-utilizing virus, we were intrigued as to whether SHIV MNA inherited the trait from the parental virus. We subjected SHIV MNA and the parental HIV-1 MNA to a co-receptor usage assay as described previously (Nishimura *et al.*, 2010), with minor modifications (Fig. S4). As expected, SHIV MNA was shown to utilize CCR5 as an entry co-receptor.

We next assessed the neutralization profiles of SHIV MNA in comparison with the parental HIV-1 MNA, as described previously (Li *et al.*, 2005; Wei *et al.*, 2002). Both SHIV MNA and HIV-1 MNA showed essentially no neutralization by KD-247 up to 25 μg ml^{-1}, and 50 % neutralization was achieved at 50 μg ml^{-1} (Fig. 1b). As the CD4 mimic, we employed YYA-021, a compound generated and characterized through studies concerning the structure–activity relationships of small molecules (Narumi *et al.*, 2010, 2011, 2013; Yamada *et al.*, 2010). The compound was shown to be slightly less potent but to exhibit substantially lower toxicity than NBD-556, and was therefore a suitable choice for our purposes in future studies in animal models. SHIV MNA was resistant to neutralization by YYA-021 at all concentrations examined, except 25 and 50 μM, and showed a neutralization profile almost identical to that of HIV-1 MNA (Fig. 1c). To further characterize the

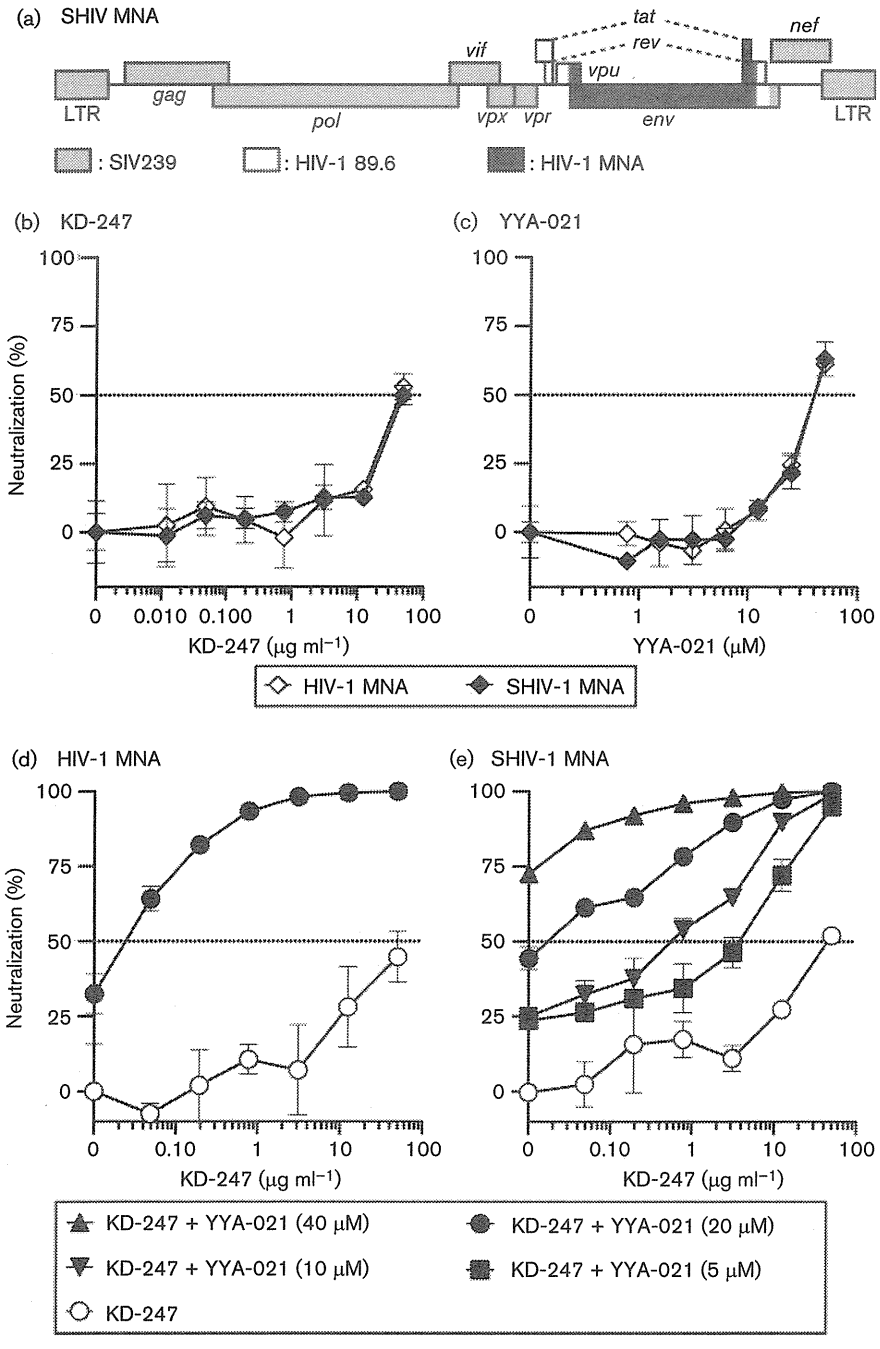

Fig. 1. Genomic organization (a) and neutralization sensitivity (b–e) of SHIV MNA. (a) Grey shaded boxes represent genes derived from SIV239, open boxes those from HIV-1 89.6 and dark grey shaded boxes those from HIV-1 MNA. LTR, long terminal repeat. (b–e) Percentage neutralization was calculated as 100×[1−(RLU.N−RLU.B)/(RLU.V−RLU.B)], where RLU is relative luciferase units; RLU.N is RLU in wells with cells, virus and KD-247 and/or YYA-021; RLU.V is RLU in wells with cells and virus; and RLU.B is RLU in wells with cells.

biological properties of SHIV MNA Env, a set of entry assays was conducted (Fig. S5). The *env* genes cloned from SHIV MNA and HIV-1 MNA were utilized to generate pseudotyped viruses. These pseudotypes were inoculated into TZM-bl cells in the presence of increasing amounts of NBD-556, YYA-021 or sCD4. A control group was derived from another virus preparation pseudotyped with amphotropic murine leukemia virus (A-MLV) Env (Landau *et al.*, 1991). When the efficiency of entry was defined by intracellular luciferase activities, virtually no difference was observed between Envs of SHIV MNA and the parental HIV-1. Thus, SHIV MNA Env replicated in

C8166-CCR5 cells retained sensitivity to small-molecule CD4 mimics and sCD4 comparable to that of HIV-1 MNA.

We then examined whether the synergistic neutralization of HIV-1 MNA by KD-247 antibody in the presence of NBD-556 (Yoshimura *et al.*, 2010) would be reproduced when CD4 mimic was substituted by YYA-021. The synergistic neutralization effect of KD-247 and YYA-021 was reproduced in our experiments (Fig. 1d). At 50 μg ml^{-1}, KD-247 barely achieved 50 % neutralization of HIV-1 MNA but resulted in 50 % neutralization at <0.05 μg ml^{-1} in the presence of 20 μM of YYA-021.

Finally, to examine whether these two agents neutralized SHIV MNA in the same manner as the parental HIV-1, we conducted a neutralization assay with KD-247 in the presence of increasing amounts of YYA-021 (0, 5, 10, 20 and 40 μM) (Fig. 1e). The neutralization curve of KD-247 against SHIV MNA showed an upward shift as the concentration of YYA-021 increased (Fig. 1e), similar to the observations with HIV-1 (Fig. 1d), indicating augmentation of neutralization, and complete neutralization of both viruses was achieved at 20 μM YYA-021 (Fig. 1d, e). Based on these results, we concluded that the neutralization profile of SHIV MNA was comparable to that of HIV-1 MNA.

Reproduction of the neutralization characteristics of HIV-1 MNA in the newly generated SHIV prompted us to assess the ability of SHIV MNA to replicate in monkey cells. SHIV MNA, along with SIV239 and SHIV KS661, were normalized with infectious titres and inoculated into rhesus macaque PBMC preparations from four animals,

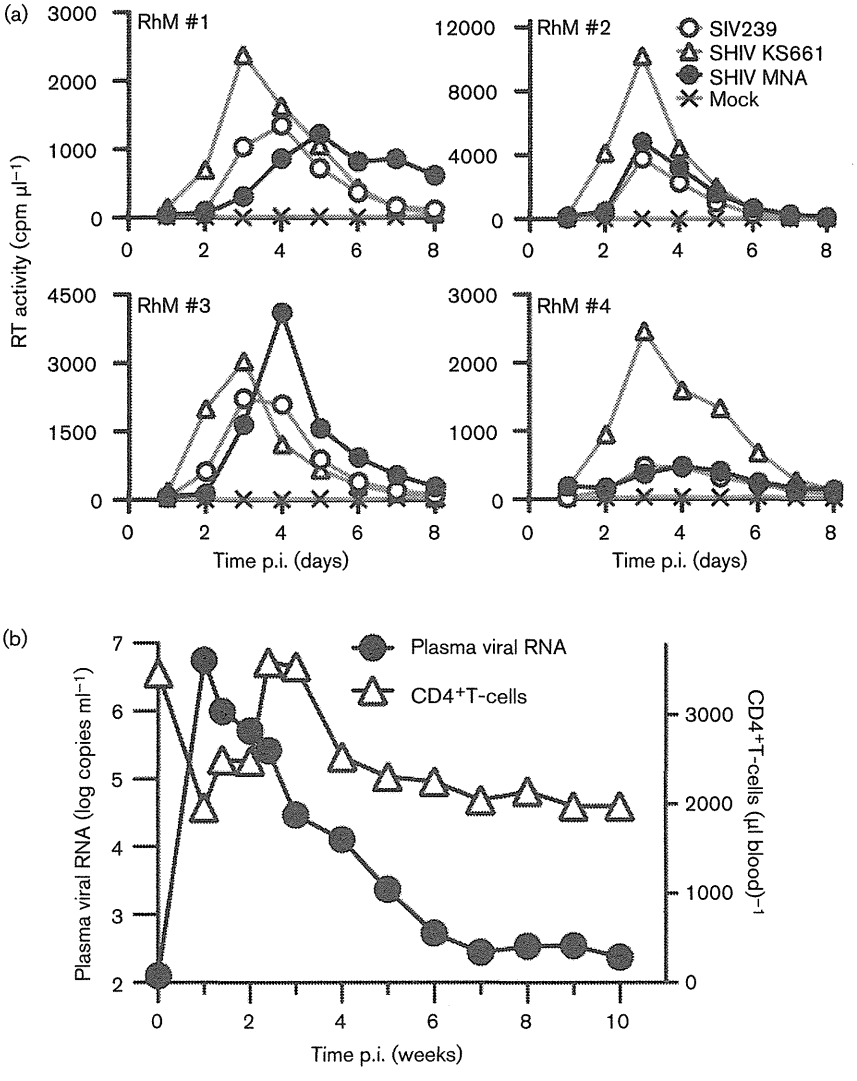

Fig. 2. Replication of SHIV MNA in rhesus macaque PBMCs (a) and *in vivo* (b). (a) M.o.i. was adjusted to 0.01 ($TCID_{50}$ per cell). (b) Experimental infection of a rhesus macaque with SHIV MNA. SHIV MNA (1.75×10^5 $TCID_{50}$) was intravenously inoculated into a rhesus macaque, and the plasma viral RNA burden and circulating $CD4^+$ T-lymphocytes were monitored.

as described previously (Fujita *et al.*, 2013) (Fig. 2a). SHIV KS661, a CXCR4-utilizing virus, replicated to the highest titres of all the viruses in all PBMC preparations. Compared with SHIV KS661, SIV239 replicated to lower titres. Under these experimental conditions, SHIV MNA showed productive replication in the cells with similar replication kinetics and peak titres to SIV239. Based on these results, we concluded that SHIV MNA was replication competent in primary monkey lymphocytes.

Productive replication of SHIV MNA in monkey PBMCs justified experimental infection of the virus *in vivo*. We inoculated 1.75×10^5 $TCID_{50}$ SHIV MNA intravenously into a rhesus macaque and monitored plasma viral RNA burden and circulating $CD4^+$ T-lymphocyte levels (Fig. 2b). Plasma viral RNA burden reached a peak of 5.6×10^6 copies ml^{-1} at 1 week post-infection (p.i.), and declined rapidly thereafter, reaching low levels of detection at 7 weeks p.i. (around 2.8×10^2 copies ml^{-1}). Circulating $CD4^+$ T-cell numbers showed a transient decrease around 1 week p.i., rebounded around 3 weeks p.i. and stabilized around 70 % of the pre-infection level from 4 weeks p.i. During the period of observation, the animal developed no obvious clinical manifestations related to lentivirus infection.

As SHIV MNA replicated *in vivo* without depleting helper T-cells, it was expected that the animal mounted an antiviral immune reaction. The production of antibody directed against Env was assessed by Western blotting, as described previously (Igarashi *et al.*, 1999). Purified Env protein (Advanced Biotechnologies) was used as the antigen (Fig. 3a). Anti-Env antibody was detected at 3 weeks p.i., and the level of antibody judged by the intensity of the band increased gradually with time.

We next examined whether the animal generated neutralizing antibodies against SHIV MNA. Because plasma samples from this specimen exhibited high background activity, IgG was purified from these samples collected on day 0 and in week 24 p.i. using protein G spin columns (GE Healthcare Japan). While the IgG from day 0 exhibited no neutralizing activity (Fig. 3b), as expected, the IgG collected at 24 weeks p.i. neutralized SHIV MNA, although a concentration >100 μg ml^{-1} was required to suppress replication of 100 $TCID_{50}$ of the input virus (Fig. 3c).

We examined whether the observed marginal neutralization by the antibody could be enhanced by the presence of YYA-021. Upon addition of YYA-021 in the assay system, SHIV MNA became sensitive to IgG obtained at 24 weeks p.i. (Fig. 3c), while no enhancement was identified from day 0 (Fig. 3b).

In this study, we generated a replication-competent SHIV MNA strain carrying an Env resistant to the neutralizing mAb KD-247 but conditionally sensitive in the presence of the CD4 mimic YYA-021. As the observed neutralization characteristics were identical to those of HIV-1 MNA, which contributed the majority of the Env sequence to the chimaera, the utility of the CD4 mimic as a means of enhancing antibody-mediated virus neutralization should be assessed in the context of infection *in vivo*. This concept could be tested during the acute phase of SHIV MNA infection, during which the virus undergoes substantial replication. To examine the feasibility of CD4-mimic-mediated enhancement of virus neutralization in the context of chronic infection, the conditions under which this type of intervention should be applied to HIV-1-infected patients in a clinical setting, the virus must be

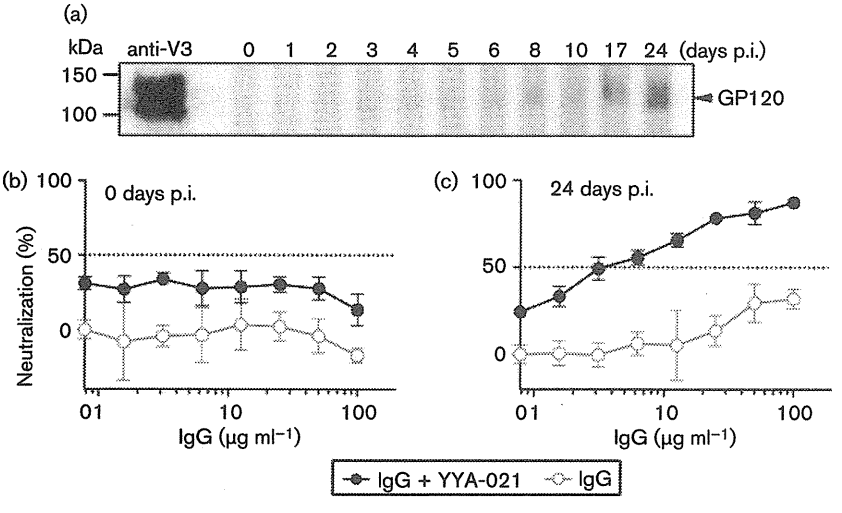

Fig. 3. Antibody induced against SHIV MNA. (a) The anti-HIV-1 gp120 antibody response was assessed by Western blotting with plasma samples collected at the indicated times. An anti-HIV-1 V3 mAb, 4G10 (ascites diluted 1 : 100) (von Brunn *et al.*, 1993), obtained from the NIH AIDS Reagent Program, was used as a positive control (lane anti-V3). (b, c) Neutralization of SHIV MNA with IgG purified from plasma of the infected rhesus macaque (day 0 and week 24 p.i.) with 20 μM YYA-021 or without YYA-021.

modified to sustain productive replication for a longer period. SHIV MNA in the present form does not fulfil this requirement. It is possible that animal-to-animal passage could increase the fitness of the virus in monkeys.

This study demonstrated that a CD4 mimic could modulate viral Env protein to be more susceptible to neutralization by less potent antibodies generated in the context of infection. During the early phase of infection, patients mount high titres of non-neutralizing antibodies directed against the V3 loop (Davis *et al.*, 2009a). Patients with HIV-1 clade C generate anti-Env antibodies, including anti-CD4i antibodies, with poor neutralizing activity against recent infection (Gray *et al.*, 2007). It is possible that the CD4 mimic YYA-021 causes a conformational change in SHIV MNA Env, which renders sequestered epitope(s) accessible to potentially neutralizing IgG, such as ones directed against the V3 loop and CD4i.

The current study extended the previous study by Yoshimura *et al.* (2010) and used HIV-1 MNA belonging to clade B to generate a new SHIV strain carrying Env. The neutralization sensitivity of this strain is characteristically augmented in the presence of a small-molecule CD4 mimic. Similar observations by Decker *et al.* (2005) showed that infections of a wide range of HIV-1 strains of multiple clades or circulating recombinant forms elicit high titres of anti-CD4i antibodies. These anti-CD4i antibodies neutralize viruses as divergent as HIV-2 in the presence of sCD4 (Decker *et al.*, 2005). Taking these observations into account, small-molecule CD4 mimics such as YYA-021 could potentially enhance the neutralization activity of the antibodies directed against autologous viruses belonging not only to clade B but also to multiple HIV-1 strains of various clades and possibly even HIV-2. Our results pave the way for a novel therapeutic intervention based on administration of CD4 mimics to patients with HIV to facilitate control of the virus by their own antibodies.

Acknowledgements

Thanks should be given to: Drs Julie Strizki and Paul Zavodny of the Schering-Plough Research Institute, Kenilworth, NJ, USA, for providing AD101; the NIH AIDS Research & Reference Reagent Program for providing TZM-bl cells, SV-A-MLV-env, 4G10 and soluble CD4; the Chemo-Sero-Therapeutic Research Institute, Kaketsuken, Japan, for providing mAb KD-247; former and current members of the Igarashi Laboratory for discussion and support. This work was supported by a Research on HIV/AIDS grant from the Ministry of Health, Labor and Welfare of Japan (H22-AIDS Research-007 and H24-AIDS Research-008) and by a Grant-in-Aid for Scientific Research (B) from the Japan Society for the Promotion of Science (23300156).

References

Davis, K. L., Bibollet-Ruche, F., Li, H., Decker, J. M., Kutsch, O., Morris, L., Salomon, A., Pinter, A., Hoxie, J. A. & other authors (2009a). Human immunodeficiency virus type 2 (HIV-2)/HIV-1 envelope chimeras detect high titers of broadly reactive HIV-1 V3-specific antibodies in human plasma. *J Virol* **83**, 1240–1259.

Davis, K. L., Gray, E. S., Moore, P. L., Decker, J. M., Salomon, A., Montefiori, D. C., Graham, B. S., Keefer, M. C., Pinter, A. & other authors (2009b). High titer HIV-1 V3-specific antibodies with broad reactivity but low neutralizing potency in acute infection and following vaccination. *Virology* **387**, 414–426.

Decker, J. M., Bibollet-Ruche, F., Wei, X., Wang, S., Levy, D. N., Wang, W., Delaporte, E., Peeters, M., Derdeyn, C. A. & other authors (2005). Antigenic conservation and immunogenicity of the HIV coreceptor binding site. *J Exp Med* **201**, 1407–1419.

Eda, Y., Takizawa, M., Murakami, T., Maeda, H., Kimachi, K., Yonemura, H., Koyanagi, S., Shiosaki, K., Higuchi, H. & other authors (2006). Sequential immunization with V3 peptides from primary human immunodeficiency virus type 1 produces cross-neutralizing antibodies against primary isolates with a matching narrow-neutralization sequence motif. *J Virol* **80**, 5552–5562.

Fujita, Y., Otsuki, H., Watanabe, Y., Yasui, M., Kobayashi, T., Miura, T. & Igarashi, T. (2013). Generation of a replication-competent chimeric simian-human immunodeficiency virus carrying env from subtype C clinical isolate through intracellular homologous recombination. *Virology* **436**, 100–111.

Gray, E. S., Moore, P. L., Choge, I. A., Decker, J. M., Bibollet-Ruche, F., Li, H., Leseka, N., Treurnicht, F., Mlisana, K. & other authors (2007). Neutralizing antibody responses in acute human immunodeficiency virus type 1 subtype C infection. *J Virol* **81**, 6187–6196.

Igarashi, T., Endo, Y., Englund, G., Sadjadpour, R., Matano, T., Buckler, C., Buckler-White, A., Plishka, R., Theodore, T. & other authors (1999). Emergence of a highly pathogenic simian/human immunodeficiency virus in a rhesus macaque treated with anti-CD8 mAb during a primary infection with a nonpathogenic virus. *Proc Natl Acad Sci U S A* **96**, 14049–14054.

Kong, L. & Sattentau, Q. J. (2012). Antigenicity and immunogenicity in HIV-1 antibody-based vaccine design. *J AIDS Clin Res* **S8**, 3.

Kwong, P. D. & Mascola, J. R. (2012). Human antibodies that neutralize HIV-1: identification, structures, and B cell ontogenies. *Immunity* **37**, 412–425.

Landau, N. R., Page, K. A. & Littman, D. R. (1991). Pseudotyping with human T-cell leukemia virus type I broadens the human immunodeficiency virus host range. *J Virol* **65**, 162–169.

Li, M., Gao, F., Mascola, J. R., Stamatatos, L., Polonis, V. R., Koutsoukos, M., Voss, G., Goepfert, P., Gilbert, P. & other authors (2005). Human immunodeficiency virus type 1 *env* clones from acute and early subtype B infections for standardized assessments of vaccine-elicited neutralizing antibodies. *J Virol* **79**, 10108–10125.

Lusso, P., Earl, P. L., Sironi, F., Santoro, F., Ripamonti, C., Scarlatti, G., Longhi, R., Berger, E. A. & Burastero, S. E. (2005). Cryptic nature of a conserved, CD4-inducible V3 loop neutralization epitope in the native envelope glycoprotein oligomer of CCR5-restricted, but not CXCR4-using, primary human immunodeficiency virus type 1 strains. *J Virol* **79**, 6957–6968.

Madani, N., Schön, A., Princiotto, A. M., Lalonde, J. M., Courter, J. R., Soeta, T., Ng, D., Wang, L., Brower, E. T. & other authors (2008). Small-molecule CD4 mimics interact with a highly conserved pocket on HIV-1 gp120. *Structure* **16**, 1689–1701.

Mascola, J. R., Stiegler, G., VanCott, T. C., Katinger, H., Carpenter, C. B., Hanson, C. E., Beary, H., Hayes, D., Frankel, S. S. & other authors (2000). Protection of macaques against vaginal transmission of a pathogenic HIV-1/SIV chimeric virus by passive infusion of neutralizing antibodies. *Nat Med* **6**, 207–210.

Moore, J. P., Cao, Y., Qing, L., Sattentau, Q. J., Pyati, J., Koduri, R., Robinson, J., Barbas, C. F., III, Burton, D. R. & Ho, D. D. (1995).

Primary isolates of human immunodeficiency virus type 1 are relatively resistant to neutralization by monoclonal antibodies to gp120, and their neutralization is not predicted by studies with monomeric gp120. *J Virol* **69**, 101–109.

Narumi, T., Ochiai, C., Yoshimura, K., Harada, S., Tanaka, T., Nomura, W., Arai, H., Ozaki, T., Ohashi, N. & other authors (2010). CD4 mimics targeting the HIV entry mechanism and their hybrid molecules with a CXCR4 antagonist. *Bioorg Med Chem Lett* **20**, 5853–5858.

Narumi, T., Arai, H., Yoshimura, K., Harada, S., Nomura, W., Matsushita, S. & Tamamura, H. (2011). Small molecular CD4 mimics as HIV entry inhibitors. *Bioorg Med Chem* **19**, 6735–6742.

Narumi, T., Arai, H., Yoshimura, K., Harada, S., Hirota, Y., Ohashi, N., Hashimoto, C., Nomura, W., Matsushita, S. & Tamamura, H. (2013). CD4 mimics as HIV entry inhibitors: lead optimization studies of the aromatic substituents. *Bioorg Med Chem* **21**, 2518–2526.

Nishimura, Y., Igarashi, T., Haigwood, N. L., Sadjadpour, R., Donau, O. K., Buckler, C., Plishka, R. J., Buckler-White, A. & Martin, M. A. (2003). Transfer of neutralizing IgG to macaques 6 h but not 24 h after SHIV infection confers sterilizing protection: implications for HIV-1 vaccine development. *Proc Natl Acad Sci U S A* **100**, 15131–15136.

Nishimura, Y., Shingai, M., Willey, R., Sadjadpour, R., Lee, W. R., Brown, C. R., Brenchley, J. M., Buckler-White, A., Petros, R. & other authors (2010). Generation of the pathogenic R5-tropic simian/human immunodeficiency virus SHIVAD8 by serial passaging in rhesus macaques. *J Virol* **84**, 4769–4781.

Platt, E. J., Wehrly, K., Kuhmann, S. E., Chesebro, B. & Kabat, D. (1998). Effects of CCR5 and CD4 cell surface concentrations on infections by macrophagetropic isolates of human immunodeficiency virus type 1. *J Virol* **72**, 2855–2864.

Shibata, R. & Adachi, A. (1992). SIV/HIV recombinants and their use in studying biological properties. *AIDS Res Hum Retroviruses* **8**, 403–409.

Shimizu, Y., Okoba, M., Yamazaki, N., Goto, Y., Miura, T., Hayami, M., Hoshino, H. & Haga, T. (2006). Construction and in vitro characterization of a chimeric simian and human immunodeficiency virus with the RANTES gene. *Microbes Infect* **8**, 105–113.

Shinohara, K., Sakai, K., Ando, S., Ami, Y., Yoshino, N., Takahashi, E., Someya, K., Suzaki, Y., Nakasone, T. & other authors (1999). A highly pathogenic simian/human immunodeficiency virus with genetic changes in cynomolgus monkey. *J Gen Virol* **80**, 1231–1240.

Thali, M., Moore, J. P., Furman, C., Charles, M., Ho, D. D., Robinson, J. & Sodroski, J. (1993). Characterization of conserved human immunodeficiency virus type 1 gp120 neutralization epitopes exposed upon gp120-CD4 binding. *J Virol* **67**, 3978–3988.

von Brunn, A., Brand, M., Reichhuber, C., Morys-Wortmann, C., Deinhardt, F. & Schödel, F. (1993). Principal neutralizing domain of HIV-1 is highly immunogenic when expressed on the surface of hepatitis B core particles. *Vaccine* **11**, 817–824.

Wei, X., Decker, J. M., Liu, H., Zhang, Z., Arani, R. B., Kilby, J. M., Saag, M. S., Wu, X., Shaw, G. M. & Kappes, J. C. (2002). Emergence of resistant human immunodeficiency virus type 1 in patients receiving fusion inhibitor (T-20) monotherapy. *Antimicrob Agents Chemother* **46**, 1896–1905.

Wyatt, R., Kwong, P. D., Desjardins, E., Sweet, R. W., Robinson, J., Hendrickson, W. A. & Sodroski, J. G. (1998). The antigenic structure of the HIV gp120 envelope glycoprotein. *Nature* **393**, 705–711.

Yamada, Y., Ochiai, C., Yoshimura, K., Tanaka, T., Ohashi, N., Narumi, T., Nomura, W., Harada, S., Matsushita, S. & Tamamura, H. (2010). CD4 mimics targeting the mechanism of HIV entry. *Bioorg Med Chem Lett* **20**, 354–358.

Yoshimura, K., Harada, S., Shibata, J., Hatada, M., Yamada, Y., Ochiai, C., Tamamura, H. & Matsushita, S. (2010). Enhanced exposure of human immunodeficiency virus type 1 primary isolate neutralization epitopes through binding of CD4 mimetic compounds. *J Virol* **84**, 7558–7568.

Yusa, K., Maeda, Y., Fujioka, A., Monde, K. & Harada, S. (2005). Isolation of TAK-779-resistant HIV-1 from an R5 HIV-1 GP120 V3 loop library. *J Biol Chem* **280**, 30083–30090.

Zhao, Q., Ma, L., Jiang, S., Lu, H., Liu, S., He, Y., Strick, N., Neamati, N. & Debnath, A. K. (2005). Identification of *N*-phenyl-*N*′-(2,2,6,6-tetramethyl-piperidin-4-yl)-oxalamides as a new class of HIV-1 entry inhibitors that prevent gp120 binding to CD4. *Virology* **339**, 213–225.

frontiers in MICROBIOLOGY

METHODS ARTICLE
published: 11 October 2013
doi: 10.3389/fmicb.2013.00298

Sensitive detection of measles virus infection in the blood and tissues of humanized mouse by one-step quantitative RT-PCR

Shota Ikeno[1,2†], Moto-omi Suzuki[1,3†], Mahmod Muhsen[1], Masayuki Ishige[1], Mie Kobayashi-Ishihara[1], Shinji Ohno[4], Makoto Takeda[5], Tetsuo Nakayama[6], Yuko Morikawa[2], Kazutaka Terahara[1], Seiji Okada[7], Haruko Takeyama[3,4] and Yasuko Tsunetsugu-Yokota[1]*

[1] Department of Immunology, National Institute of Infectious Diseases, Tokyo, Japan
[2] Cooperative Major in Advanced Health Science, Tokyo University of Agriculture and Technology/Waseda University Graduate School of Collaborative Education Curriculum, Tokyo, Japan
[3] Department of Life Science and Medical Bioscience, Graduate School of Advanced Science and Engineering, Waseda University, Tokyo, Japan
[4] Department of Virology, Faculty of Medicine, Kyushu University, Fukuoka, Japan
[5] Department of Virology III, National Institute of Infectious Diseases, Tokyo, Japan
[6] Kitasato Institute for Life Science, Kitasato University, Tokyo, Japan
[7] Division of Hematopoiesis, Center for AIDS Research, Kumamoto University, Kumamoto, Japan

Edited by:
Akio Adachi, The University of Tokushima Graduate School, Japan

Reviewed by:
Takashi Irie, Graduate School of Biomedical Sciences, Hiroshima University, Japan
Masato Tsurudome, Mie University Graduate School of Medicine, Japan
Masae Itoh, Nagahama Institute of Bio-Science and Technology, Japan

***Correspondence:**
Yasuko Tsunetsugu-Yokota, Department of Immunology, National Institute of Infectious Diseases, 1-23-1 Toyama, Shinjuku, Tokyo 162-8640, Japan
e-mail: yyokota@nih.go.jp

†Shota Ikeno and Moto-omi Suzuki have contributed equally to this work.

Live attenuated measles virus (MV) has long been recognized as a safe and effective vaccine, and it has served as the basis for development of various MV-based vaccines. However, because MV is a human-tropic virus, the evaluation of MV-based vaccines has been hampered by the lack of a small-animal model. The humanized mouse, a recently developed system in which an immunodeficient mouse is transplanted with human fetal tissues or hematopoietic stem cells, may represent a suitable model. Here, we developed a sensitive one-step quantitative reverse transcription (qRT)-PCR that simultaneously measures nucleocapsid (N) and human RNase P mRNA levels. The results can be used to monitor MV infection in a humanized mouse model. Using this method, we elucidated the replication kinetics of MV expressing enhanced green fluorescent protein both *in vitro* and in humanized mice in parallel with flow-cytometric analysis. Because our qRT-PCR system was sensitive enough to detect MV expression using RNA extracted from a small number of cells, it can be used to monitor MV infection in humanized mice by sequential blood sampling.

Keywords: measles virus infection, humanized mouse, quantitative RT-PCR, EGFP expression, flow cytometry

INTRODUCTION

Measles, a highly contagious childhood disease caused by the measles virus (MV), affects more than 20 million people each year. MV infection is characterized by a high fever with typical Koplik's spots followed by the appearance of a generalized maculopapular rash, and is often associated with respiratory and neuronal complications (Griffin, 2007). Since the implementation of vaccination programs using an effective live attenuated MV vaccine, global measles deaths have decreased dramatically. Nevertheless, measles is still one of the leading causes of death among young children under the age of 5 years, especially in countries with weak health infrastructures, and approximately 158,000 measles death occurred in 2011 (http://www.who.int/mediacentre/factsheets/fs286/en/). The ongoing global vaccination strategy aims to protect small children at high risk.

The MV vaccine is safe, effective, and inexpensive. Based on its long and successful vaccination history, several groups have taken advantage of reverse-genetics technology to utilize the live attenuated MV vaccine strain as a viral vector to elicit immune responses against foreign antigens from various pathogens, such as Env or Gag of human immunodeficiency virus (HIV; Lorin et al., 2004; Stebbings et al., 2012), hepatitis B surface (S) antigen (Singh et al., 1999; Reyes-del Valle et al., 2009), fusion protein of respiratory syncytial virus (Sawada et al., 2011), and envelope glycoprotein of West Nile virus (Despres et al., 2005; Brandler et al., 2012). MV is a human-tropic virus that uses CD46, signaling of lymphocyte activation molecule (SLAM, CD150), and the recently identified epithelial-cell receptor nectin-4 (PVRL4, see review in Kato et al., 2012) as receptors. To test the immune response against MV-based recombinant vaccines, both MV receptor-transgenic mice (Singh et al., 1999; Lorin et al., 2004; Despres et al., 2005) and non-human primates have been used as animal models (Reyes-del Valle et al., 2009; Brandler et al., 2012; Stebbings et al., 2012).

Although non-human primates are susceptible to MV, and they develop pathologies similar to those that occur in humans, the expense of using monkeys in research limits the number of animals that can be used for studies. To overcome such practical problems, various types of human MV receptor-transgenic mice expressing CD46 or CD150 have been developed (review in

Sellin and Horvat, 2009). Unfortunately, MV infection of all of these human MV receptor-expressing mouse models is severely restricted by the presence of murine type I IFN; to establish MV infection, it is necessary to introduce the IFNα receptor knockout into the MV receptor-transgenic mice, even in strains expressing CD150 driven by a native human promoter (Ohno et al., 2007). The IFNα receptor knockout/CD150 knock-in mouse is highly susceptible to MV infection and reproduces some aspects of MV infection in humans, including immunosuppression (Koga et al., 2010). This makes it a useful mouse model for study purposes. However, one problem is the lack of an initial innate immune response, which may modify the outcome of MV infection. Thus, the model may not truly reflect the outcome in humans.

In the early 2000s, a series of immunodeficient mice were developed that allow efficient transplantation of human cells or tissues; these systems are collectively termed "humanized mice." A large number of studies have described the development of human hematopoietic cells and their immunological functions in humanized mice, and technical modifications have been made for the study of various human diseases (Ito et al., 2012). Currently, humanized mouse systems are widely used as alternatives to non-human primate models, especially for the study of human-tropic infectious diseases such as HIV, human T cell leukemia virus (HTLV), dengue virus, HCV, and EB virus (Akkina, 2013). Of the different humanized mice models, the BM/Liver/Thymus transplanted (BLT) mouse, which is transplanted with human fetal liver and thymus tissue in addition to hematopoietic stem cells (HSCs), is recognized as the model that most closely mimics the human immune response (Wege et al., 2008). However, the use of this model is limited, mainly because of the ethical issues surrounding human fetal organs/tissues.

We have recently established an HIV infection model in NOD/SCID/Jak3null (NOJ) mouse transplanted with human cord blood HSCs (Terahara et al., 2013). To study MV infection in humanized NOJ (hNOJ), we infected an MV vaccine strain (AIK-C) expressing enhanced green fluorescent protein (EGFP) into hNOJ and analyzed the MV-infected cells by flow cytometry. The hNOJ mouse is highly susceptible to MV infection; in that study, we observed that GFP^+ cells were present in systemic lymphoid tissues and bone marrow (BM). Because it is important to assess MV infection kinetics in an animal without sacrificing the infected mouse, we developed a highly sensitive one-step quantitative reverse transcription-PCR (qRT-PCR) system to monitor MV infection in human peripheral blood mononuclear cells (PBMCs) circulating in the blood of humanized mice. In this study, we describe how this monitoring system works and demonstrate that the results obtained reflect the actual frequency of MV-infected cells, as determined by flow cytometry.

MATERIALS AND METHODS

CELL FRACTIONATION OF PBMCs

Peripheral blood mononuclear cells were obtained from human blood samples of healthy volunteers. Samples were collected after obtaining the approval of the institutional ethical committee of the National Institute of Infectious Diseases (NIID; No. 350) and written informed consent from each subject. PBMCs were separated by Ficoll–Hypaque density-gradient centrifugation (Lymphosepal; IBL, Gunma, Japan).

To obtain monocyte-derived dendritic cells (MDDCs), monocytes were enriched from PBMCs using CD14 microbeads (Miltenyi Biotec) and cultured in RPMI 1640 supplemented with 10% fetal bovine serum (FBS), 2 mM glutamine, and antibiotics in the presence of interleukin-4 (IL-4) and granulocyte–macrophage colony-stimulating factor (GM-CSF; both 10 ng/ml, from PeproTech Inc., London, UK) for 1 week. T cells were isolated from CD14-negative PBMCs using the Total T Cell Enrichment Kit (STEMCELL technologies, Vancouver, BC, Canada).

PREPARATION OF RNA

Total RNA was extracted from mouse blood, BM, and spleen of humanized mice, human PBMCs, and Jurkat cells expressing human SLAM (Jurkat/hSLAM) using the RNeasy Mini Kit (QIAGEN, Valencia, CA, USA) or the Total RNA Isolation Mini Kit (Agilent Technologies, Santa Clara, CA, USA).

To prepare a standard of MV RNA, the cDNA encoding measles virus nucleocapsid (N) (MV-N: AB052821) was subcloned into the pBluescript II vector, and then MV-N RNA was produced by *in vitro* RNA transcription using the T7 RiboMAX^{TM} Express Large Scale RNA Production System (Promega, Madison, WI, USA). The RNA product was purified by DNase treatment, followed by phenol–chloroform extraction and ethanol precipitation, according to the protocol supplied by the manufacturer. The final concentration of RNA was measured using an ND-1000 spectrophotometer (Thermo, Waltham, MA, USA).

PREPARATION OF STANDARD TEMPLATE DNA

To prepare a standard template DNA, cDNAs of human CD45 (hCD45: NG_007730) and RNase P (NM_006413) were synthesized from total RNA of CEM cells by reverse transcription (RT)-PCR using SuperScript III RT/Platinum Taq Mix (Invitrogen, Carlsbad, CA, USA). The products were further amplified by PCR using TaKaRa Ex Taq Hot Start Version (TAKARA, Otsu, Shiga, Japan) for hCD45, or AmpliTaq Gold 360 (Applied Biosystems, Carlsbad, CA, USA) for RNase P. These PCR products of hCD45 and RNase P were subcloned into plasmids using the pGeneBLAzer TOPO TA Expression kit (Invitrogen) and pGEM-T (Easy) Vector Systems (Promega), respectively.

REAL-TIME RT-PCR ASSAY

To perform real-time qRT-PCR, SuperScript III Platinum One-Step Quantitative RT-PCR system (Invitrogen) was used according to the manufacturer's instructions. Briefly, each reaction contained 1× reaction mix, ROX reference dye, SuperScript III RT/Platinum TaqMix, 0.2 μM specific primers, and 0.1 μM TaqMan probe. Reactions were performed on an Mx3000P qPCR system (Agilent Technologies). Thermocycling parameters included a RT step at 50°C for 20 min, followed by a DNA polymerase activation step at 95°C for 2 min and 50 PCR cycles (95°C for 20 s, 60°C for 30 s). Threshold cycle (C_t) values were calculated for each reaction; C_t represents the cycle at which a statistically significant increase in the emission intensity of the reporter relative to the passive reference dye is first detected.

For detection of hCD45 mRNA, the following sequences were used: forward primer, 5′-GGA AGT GCT GCA ATG TGT CAT T-3′; reverse primer; 5′-CTT GAC ATG CAT ACT ATT ATC TGA TGT CA-3′; TaqMan probe; 5′-FAM-ACA ACT AAA AGT GCT CCT CCA AGC CAG GTC T-BHQ1-3′ (Hamaia et al., 2001). For detection of RNase P mRNA: forward primer, 5′-AGA TTT GGA CCT GCG AGC G-3′; reverse primer, 5′-GAG CGG CTG TCT CCA CAA GT-3′; TaqMan probe, 5′-FAM-TTC TGA CCT GAA GGC TCT GCG CG-BHQ1-3′ (Kimberly et al., 2005). For detection of MV-N RNA: forward primer, 5′-CGA TGA CCC TGA CGT TAG CA-3′; reverse primer, 5′-GCG AAG GTA AGG CCA GAT TG-3′; TaqMan probe, 5′-FAM-AGG CTG TTA GAG GTT GTC CAG AGT GAC CAG-BHQ1-3′ (Hummel et al., 2006).

GENERATION OF HUMANIZED MICE

Humanized NOD/SCID/JAK3null mice were established as described previously (Terahara et al., 2013). In brief, NOJ mice were transplanted with human HSCs ($0.5–1 \times 10^5$ cells) enriched from human umbilical cord blood cells into the livers of irradiated (1 Gy) newborn mice within 2 days after birth. All mice were maintained under specific pathogen-free conditions in the animal facility at NIID and were treated in accordance with the guidelines issued by the Institutional Animal Care and Committee of NIID.

Human umbilical cord blood was donated by the Tokyo Cord Blood Bank (Tokyo, Japan) after obtaining informed consent. The use of human umbilical cord blood cells was approved by the Institutional Ethical Committees of NIID and the Tokyo Cord Blood Bank. Human HSCs were isolated using the CD133 MicroBeads Kit (Miltenyi Biotec, Bergisch Gladbach, Germany). The purity was approximately 90% as assessed by flow cytometry.

PREPARATION AND INFECTION OF MV

Recombinant wild-type MV (IC323: AB016162) expressing EGFP (IC323-EGFP; Hashimoto et al., 2002) and a recombinant vaccine strain of MV (AIK-C: S58435) expressing EGFP (AIK-C-EGFP; Fujino et al., 2007) were grown in Vero/hSLAM cells. Virus titers were determined by plaque assay using Vero/hSLAM cells.

Jurkat/hSLAM cells were infected with various doses of MV [multiplicity of infection (MOI) = 0.25, 0.05, and 0.01] by incubation at 37°C for 1 h, washed twice with phosphate buffered saline (PBS), and seeded on 24-well plates. Cells were harvested immediately after washing (time 0) or 6, 12, 18, or 24 h later. The harvested cells were either lysed for RNA extraction or analyzed by flow cytometry.

Humanized NOD/SCID/JAK3null mice were challenged intravenously (i.v.) with different doses [200, 2,000, 10,000, or 20,000 plaque-forming units (pfu)] of AIK-C-EGFP. Peripheral blood was obtained from MV-infected hNOJ mice at 3, 5, 7, 10, 14, and 21 days post-infection (p.i.). In some experiments, MV-infected hNOJ mice were sacrificed at day 7 p.i. At the time of sacrifice, peripheral blood, BM, spleen, and mesenteric lymph nodes (MLNs) were harvested, and red blood cells were lysed in ACK buffer (0.15 M NH_4Cl, 1 mM $KHCO_3$, and 0.1 mM EDTA-2Na; pH 7.2–7.4).

FLOW-CYTOMETRIC ANALYSIS OF MV-INFECTED CELLS

PE-conjugated anti-human CD150 (A12) and Pacific Blue-conjugated anti-hCD45 (HI30) monoclonal antibodies (mAbs) were purchased from BioLegend Inc. (San Diego, CA, USA). Cells were stained with these mAbs, fixed with 2% formalin/PBS for 15 min at room temperature, washed, and kept at 4°C prior to flow-cytometric analysis. Dead cells were stained with a LIVE/DEAD Fixable Dead Cell Stain Kit (L34957; Invitrogen). Data were collected using a FACScanto (BD Biosciences, San Jose, CA, USA) and analyzed using the FACSDiva (BD Biosciences) or FlowJo (Tree Star, San Carlos, CA, USA) software.

STATISTICAL ANALYSIS

Non-parametric one-way ANOVA was performed to compare cell type-specific differences in hCD45 and RNase P mRNA expression. Spearman's rank correlation coefficient test was also performed to compare the level of MV-N expression and frequency of MV-infected cells. Prism ver.5 software (GraphPad Software, San Diego, CA, USA) was used for all analyses. $P < 0.05$ was considered statistically significant.

RESULTS

HUMAN-SPECIFIC qRT-PCR SYSTEM FOR THE DETECTION OF MV INFECTION

For the detection of MV infection in clinical specimens, Hummel et al. (2006) established a sensitive qRT-PCR system that used primer and probe sets targeting the MV-N gene. In our humanized mouse model, it is necessary to analyze endogenous mRNA expression in human PBMCs to determine the level of human cell-associated MV infection in mouse blood. We initially assumed that hCD45 expression would be suitable to discriminate human hematopoietic cells from co-existing mouse hematopoietic cells *in vivo*. On that basis, we designed human-specific primer and TaqMan probe sets for hCD45 and compared their usefulness with a primer/probe set for a widely used housekeeping gene, RNase P. RNA was extracted from humanized (hu-mouse) or non-humanized (non-hu-mouse) murine splenocytes, and the level of mRNA was measured by one-step qRT-PCR. Both hCD45 and RNase P primer/probe sets detected mRNA expression of target genes from human PBMCs present in hu-mouse spleen, at similar sensitivities, but neither set detected expression in non-hu-mouse (**Figure 1A**). Thus, both primer/probe sets are human-specific. Next, we enriched $CD14^+$ monocytes and T cells from PBMCs by positive and negative magnetic-bead selection, respectively, and then determined the copy numbers of hCD45 and RNase P in these cell fractions from each of five donors. In **Figure 1B**, the expression levels of hCD45 (left panel) and RNase P (right panel) in monocytes and T cells are depicted relative to the level in each donor's PBMCs. Because RNase P expression was less affected by cell type than CD45 expression ($^*P < 0.05$), in subsequent experiments we exclusively used RNase P primer/probe sets as an endogenous control for mRNA expression.

PARALLEL INCREASE IN THE TIME COURSE OF MV-INFECTED CELL FREQUENCY AND MV-N RNA LEVEL *IN VITRO*

Because wild-type MV mainly utilizes SLAM as the receptor for entry into lymphoid cells (Tatsuo et al., 2000), the kinetics of MV

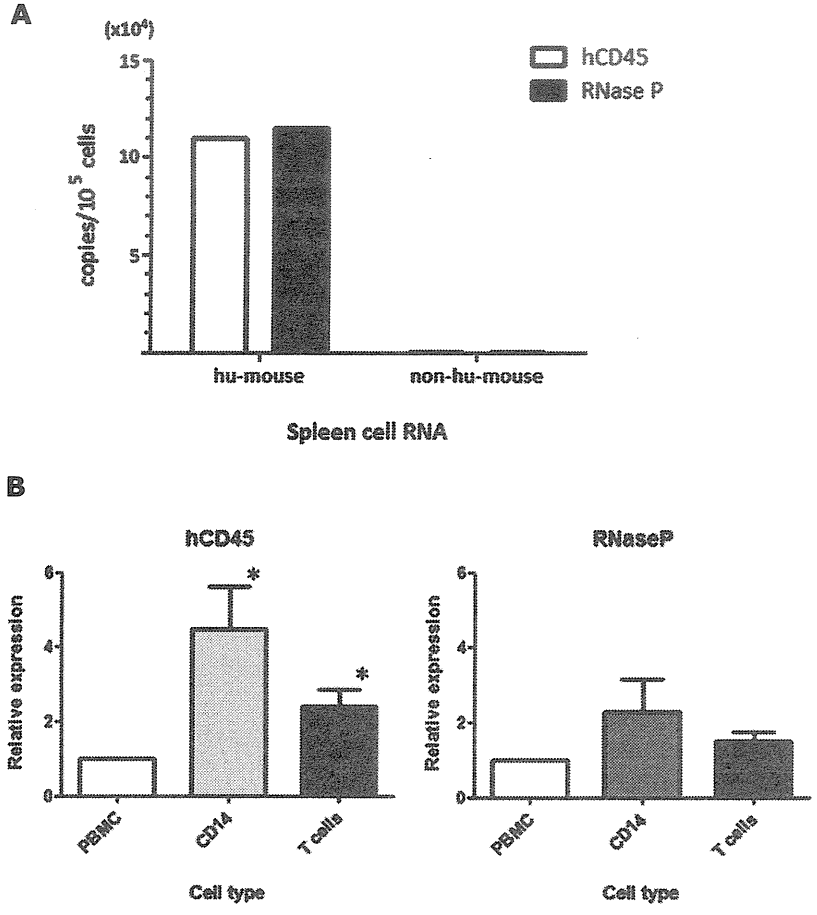

FIGURE 1 | Selection of an endogenous control for the analysis of MV-infected human PBMCs. (A) RNA was extracted from spleen cells of hNOJ and non-humanized NOJ, and one-step qRT-PCR was performed using primer and probe sets designed against the human-specific hCD45 and RNaseP mRNAs. To calculate copy numbers of these genes, the PCR products of human CD45 and RNase P were subcloned into plasmids and used as standard DNAs. **(B)** Human PBMCs from five donors were fractionated into $CD14^+$ monocytes and T cells. RNA from these cell populations was extracted, and the expression levels of hCD45 and RNase P were analyzed by qRT-PCR. The graph depicts the expression levels in these fractionated cells relative to the levels in PBMCs (defined as 1). Statistical differences in hCD45 and RNase P expression among these cell populations were evaluated by non-parametric one-way ANOVA test ($^*P<0.05$).

infection in Jurkat/hSLAM cells can be clearly visualized by flow cytometry. We infected Jurkat/hSLAM cells with a wild-type MV encoding EGFP (IC323-EGFP) at MOI of 0.01, 0.05, and 0.25. Cells were washed and harvested at 6, 12, 18, or 24 h after MV infection. A subset of the cells in each sample was analyzed by flow cytometry, and the remainder of the sample was used for RNA extraction. The mRNA levels of MV-N and RNase P were determined by qRT-PCR, and the level of MV-N mRNA relative to RNase P RNA was calculated. Representative results of three experiments are shown in **Figure 2A** (flow cytometry) and **Figure 2B** (qRT-PCR). Because of the rapid and strong cytopathic effect by MV at the highest MOI (0.25), we omitted the flow cytometry data corresponding to that condition. At MOI 0.01, a similar frequency of GFP^+ cells was detectable at 12 and 18 h p.i., whereas at MOI 0.05, the GFP^+ cell frequency was already high at 12 h p.i. Note that the level of hSLAM was not down-modulated by MV infection. Over the time course, relative MV-N expression level at all three MOIs increased in parallel over two orders of magnitude, indicating that these two methods yield comparable results (as shown in **Figure 2C**) and are useful for monitoring the replication kinetics of MV infection *in vitro*.

PARALLEL INCREASE OF MV-INFECTED CELL FREQUENCY AND MV-N RNA LEVELS *IN VIVO*

We then applied these detection systems *in vivo* in MV-infected hNOJ mice. hNOJ mice were infected with an MV vaccine strain expressing EGFP (AIK-C-EGFP) at 2000 pfu, and the animals were sacrificed 7 days later. Blood PBMCs and BM cells were washed with PBS, and a subset of the cells in each sample were stained with anti-hCD45 mAb. Representative results of flow-cytometric analysis of BM cells from three mice are shown in **Figure 3A**. The percentages of GFP^+ cells in mice 127-1, 127-4, and 127-5 mice were low (0.002%), high (0.35%), and intermediate (0.028%), respectively. The number of human PBMCs obtained from mouse blood was not sufficient to determine GFP^+

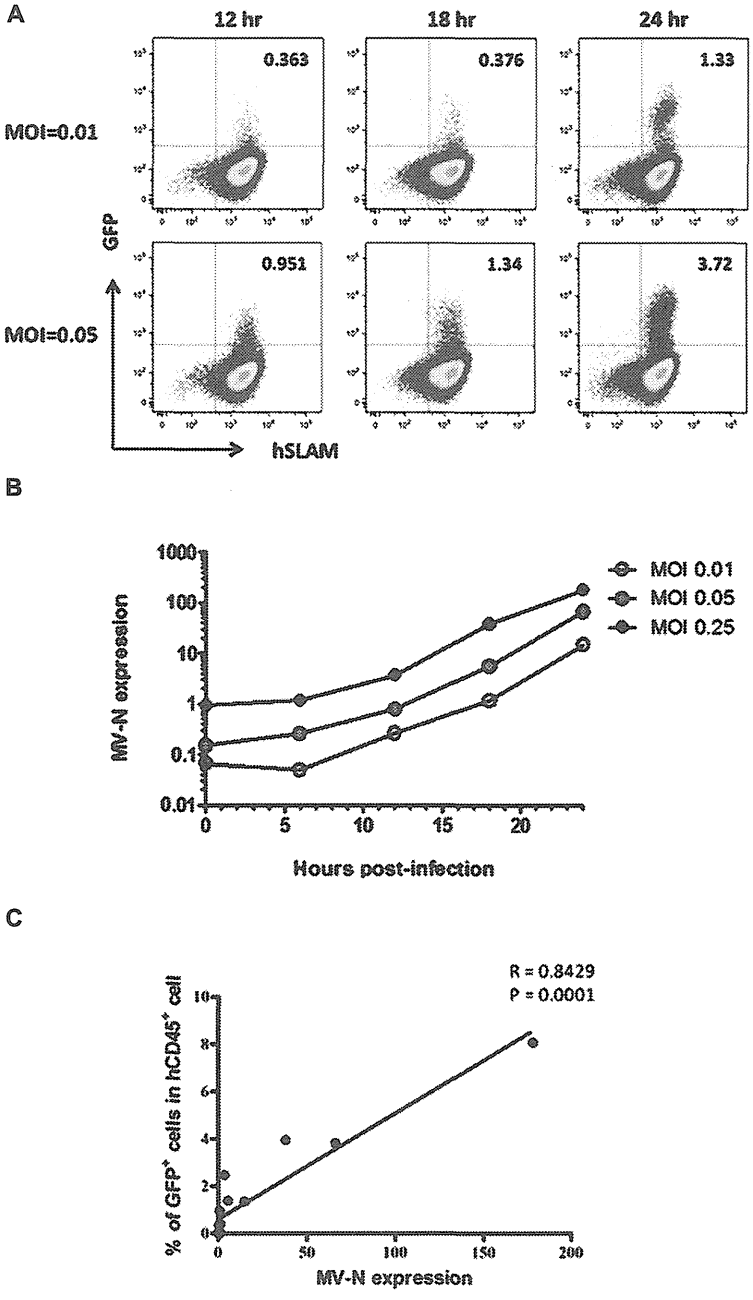

FIGURE 2 | Time course of MV infection *in vitro*. Jurkat/hSLAM cells were infected with wild-type MV IC323-EGFP at MOI of 0.01, 0.05, and 0.25, washed, and harvested at the indicated time points. **(A)** Cells were stained with PE-conjugated anti-hSLAM mAb, fixed with 2% formalin/PBS, and GFP expression was analyzed. **(B)** RNA was extracted from cells, and expression levels of MV-N and RNase P were analyzed by one-step qRT-PCR. The copy numbers of MV-N and RNase P were determined, and the ratio of MV-N copies to RNase P copies is depicted on the vertical axis. **(C)** Correlation between the percentage of GFP^+ Jurkat/SLAM cells and the time course of MV-N expression. Spearman's rank correlation coefficient was used for statistical analysis.

cell frequencies by flow cytometry. Next, we extracted RNA from PBMCs and BM cells and analyzed MV-N expression by qRT-PCR, as described in the previous section. MV-N expression paralleled the GFP^+ frequencies in BM (**Figure 3B**). Notably, a high level of MV-N expression was also detected in PBMCs of mouse 127-4, suggesting that the level of MV-N expression per single hematopoietic cell is similar between blood and BM. We plotted the GFP^+ frequency and MV-N expression level in BM cells of eight mice. As shown in **Figure 3C**, these values were well correlated ($R = 0.9286$). Taken together, these data indicate that MV infection *in vivo* is detectable in BM by both flow cytometry and MV-N RNA qRT-PCR analysis, but only MV-N RNA qRT-PCR is

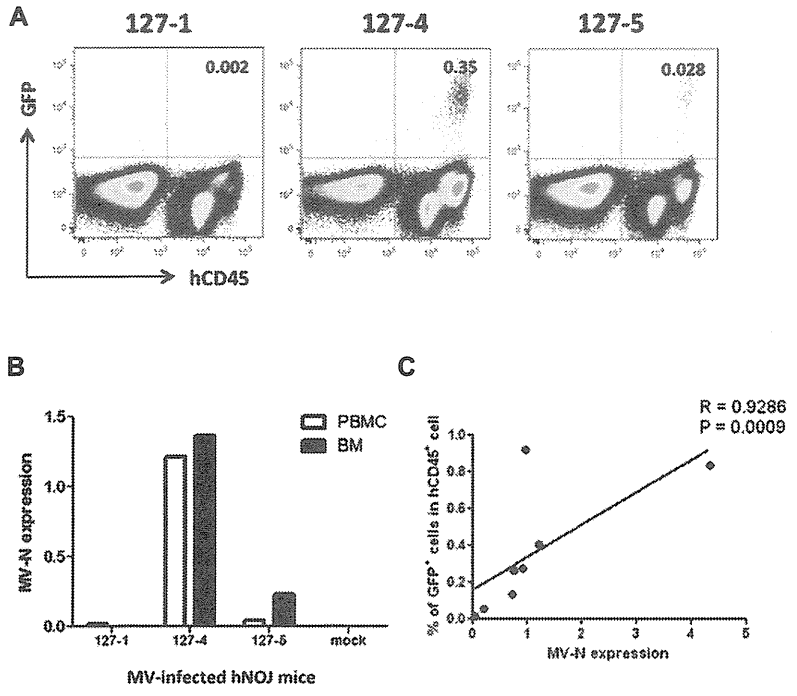

FIGURE 3 | Analysis of MV infection *in vivo*. Three hNOJ mice (127-1, -4, and -5) were infected intravenously with 2,000 pfu of the MV vaccine strain, AIK-C-EGFP. Mice were sacrificed at day 7 post-infection, and blood and bone marrow cells (BM) were obtained. **(A)** BM cells were stained with PB-anti-human CD45 mAb, fixed with 2% formalin/PBS, and GFP expression was analyzed. **(B)** PBMCs from blood and BM cells were lysed, and RNA was prepared. The expression MV-N and RNase P was analyzed as described in the legend for **Figure 2B**. **(C)** Correlation between the percentage of GFP^+ cells among $hCD45^+$ cells in BM and the level of MV-N expression in MV-infected hNOJ mice, at day 7 ($n = 4$) or day 10 ($n = 4$) p.i. Spearman's rank correlation coefficient was used for statistical analysis.

sensitive enough to detect PBMC-associated MV infection in the blood.

KINETICS OF MV GROWTH CAN BE MONITORED IN THE BLOOD OF hNOJ MOUSE

Finally, we measured MV growth kinetics *in vivo* by qRT-PCR analysis using sequential blood samples obtained from MV-infected hNOJ mice; it was not feasible to perform these measurements by flow cytometry because of the paucity of human PBMCs in the blood. Two or three hNOJ mice in each group were infected intravenously with 200, 2000, or 20,000 pfu AIK-C-EGFP and followed up to 21 days p.i. The level of PBMC-associated MV RNA in individual mice is shown in **Figure 4A**. We noticed two peaks of MV replication, the first at around day 3 p.i., and the second at day 10 p.i., irrespective of the initial inoculum. Two mice infected with 20,000 pfu MV exhibited a high level of MV replication that peaked at day 10 p.i. One mouse infected with 2,000 pfu exhibited a high level of MV replication at day 3 p.i., followed by a small peak at day 10 p.i. For some mice, we counted the number of human cells per 50 μl of blood used for RNA extraction. The data are shown in **Figure 4B**. We were able to detect high levels of MV in samples containing less than 2,000 cells, indicating that the qRT-PCR system is sensitive enough to detect low numbers of MV-infected human cells.

Although MV replication was not obvious in three mice infected with the smallest dose (200 pfu), one of these animals exhibited an increase in MV RNA expression at day 21 p.i. (gray circle). We sacrificed this particular mouse and used flow cytometry to analyze GFP expression in its blood, spleen, MLN, and BM. As shown in **Figure 4C**, GFP^+ cells were present in spleen (0.308%) and all the other tissues, albeit at a lower frequency, indicating that MV infection can occur even at a low dose (200 pfu) and spread slowly in the systemic lymphoid tissues of hNOJ.

It may be necessary to acquire at least 30,000 events to be sure of having >10,000 cells for flow cytometry analysis. This is because of the substantial amount of sample loss that occurs in this system. The flow cytometry data presented in **Figure 4C** were obtained by analyzing ~0.4 ml blood from a sacrificed mouse. However, even under these conditions, the proportion of MV-infected cells detected was only 0.056%; indeed, the cells are barely visible on the plot. Therefore, it appears that flow cytometry is not a suitable method for the sequential monitoring of infected (GFP^+) cells. Thus, the qRT-PCR system we have developed here allowed us to monitor systemic MV replication using a small volume of blood from humanized mice.

DISCUSSION

Based on a highly sensitive MV-N RNA detection method previously developed by Hummel et al. (2006), which could detect one copy of synthetic MV RNA/reaction, we developed a novel one-step real-time qRT-PCR system for the purpose of monitoring MV replication in the blood of MV-infected humanized mice.

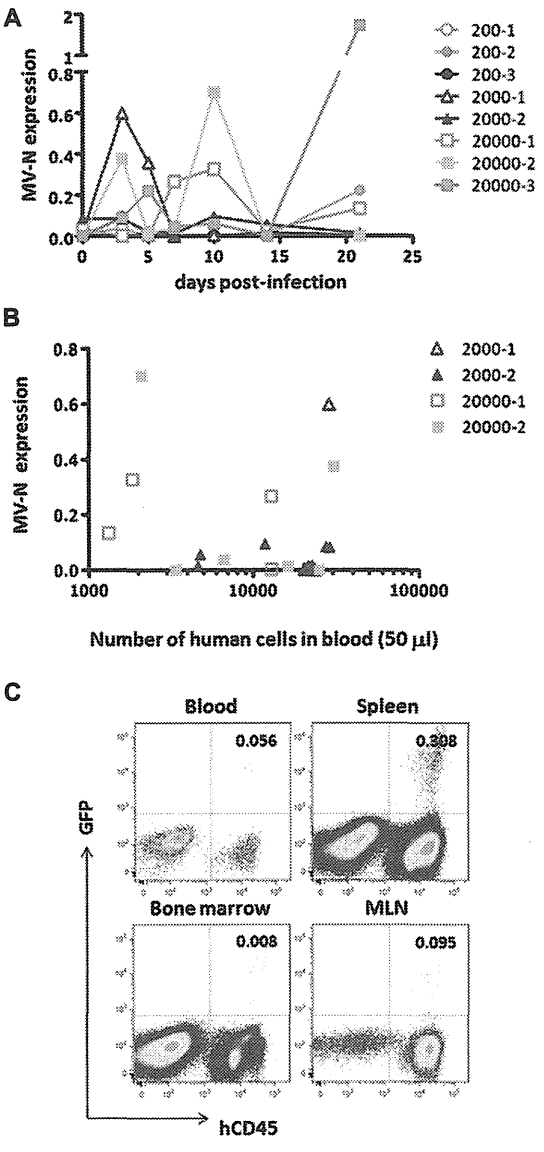

FIGURE 4 | Monitoring of MV replication *in vivo*. Two to three hNOJ mice per group were challenged with MV AIK-C-EGFP at 20,000 (squares), 2,000 (triangles), or 200 pfu (circles). The PBMCs of these mice were collected at day 3, 5, 7, 10, 14, and 21 p.i. **(A)** The level of MV-N expression in the blood of infected hNOJ. Vertical axis shows the level of MV-N relative to that of RNaseP, as described in the legend for **Figure 2B**.**(B)** For some mice (depicted using the same symbol as **(A)**), the number of human cells per 50 μl of blood used for RNA extraction and analyzed for MV-N expression was plotted on the X-axis. **(C)** An hNOJ mouse infected with MV at a low dose (gray closed circle, 200-2) exhibited an increased level of MV-N. At day 21 p.i., the mouse was sacrificed; cells from blood, spleen, BM, and mesenteric lymph node (MLN) were prepared. Cells were stained and analyzed as described in the legend for **Figure 2A**.

Because MV replication usually occurs in association with cells (Griffin, 2007), it is necessary to evaluate the endogenous RNA expression level of human PBMCs that co-exist with mouse blood cells. To this end, we designed human-specific primer/probe sets for the CD45 and RNase P mRNAs. When we analyzed the detection efficiencies of these two primer/probe sets using distinct cell types present in human PBMCs, we found that RNase P expression was less dependent than CD45 expression on cell type. Using this qRT-PCR system with RNase P as an internal control, we can reliably detect MV replication with high sensitivity in humanized mice *in vivo*. When MV expressing GFP was used for infections *in vitro* or *in vivo*, the level of MV-N RNA was closely correlated with the frequencies of GFP^+ MV-infected cells determined by flow cytometry.

Our qRT-PCR system allowed us to follow MV replication *in vivo* using a small amount of blood, with no need to sacrifice mice at each time point. Although flow-cytometric analysis provides valuable information, such as the proportions of various cell types and the surface phenotypes of MV-infected cells, the small number of human cells circulating in the mouse blood may not be sufficient for precise estimation of MV-infected cells by flow cytometry. By contrast, our qRT-PCR system was able to detect MV-N RNA in fewer than 2,000 human PBMCs (**Figure 4B**). This is an important technological advantage considering that individual humanized mice exhibit variable levels of human cell engraftment, i.e., chimerism (Terahara et al., 2013); moreover, there may exist donor-to-donor variation in susceptibility to MV infection. Thus, it should be possible to select humanized mice with a degree of MV infection appropriate for the purpose of a given experiment.

In this study, MV was inoculated through the tail vein, and infected cells were distributed to systemic lymphoid tissues as well as BMs, where human hematopoietic cells localize in humanized mice (Traggiai et al., 2004). MV may also be distributed to other organs, such as lung and intestinal tissue, as demonstrated in the case of HIV infection using the BLT mouse (Sun et al., 2007). To our surprise, by monitoring MV replication in PBMCs of humanized mice, we noticed two peaks of MV replication, at around 3 and 10 days p.i., in some mice. This pattern of MV replication did not depend on the initial dose of MV inoculum. We do not know why MV replication showed two peaks in many animals. However, it was recently reported in a monkey model that MV RNA persists in PBMCs for more than 1 month after primary infection, and declined in three phases (Lin et al., 2012). The authors of that study hypothesized that both T cells, including regulatory T cells (Treg), and antibody responses contributed to the dynamics of MV replication *in vivo*. Although hNOJ mice are reported to show poor immune responses, the role of regulatory T cells should be considered. This is because these cells regulate HIV-1 infection in humanized mice (Jiang et al., 2008). Alternatively, it may be that the intravenous injection of MV rapidly kills the target cells (probably those showing an activated phenotype) within 3 days. The low number of MV-infected cells then gradually transmits the virus to the human cells that are replenished from the BM stem cell pool. Further investigations are required to clarify this issue.

The humanized mouse model is expected to be a useful tool for studying virus infection (Akkina, 2013). Although the human immune system is not fully reconstructed by the transplantation of human HSCs alone, we believe that further improvements are possible, which will allow us to utilize this mouse model to not only evaluate vaccine and drug efficacy but also to increase our understanding of the pathogenesis of MV infection. The described novel method of monitoring MV-infected human cells in the blood will

be useful for studying MV-based vaccines in humanized mouse models without the need to sacrifice the mice.

ACKNOWLEDGMENTS

We thank Prof. Yusuke Yanagi for providing IC323-EGFP, and Ms. Kahori Okano for her excellent technical assistance. We also thank the Tokyo Cord Blood Bank for donating human umbilical cord blood. This work was supported in part by a grant from the Ministry of Health, Labor, and Welfare of Japan, and in part by a grant from the Ministry of Education, Science, Sports, and Culture of Japan. Shota Ikeno is supported by the Global COE Program (Practical Chemical Wisdom) from the Ministry of Education, Culture, Sports, Science, and Technology of Japan.

REFERENCES

Akkina, R. (2013). New generation humanized mice for virus research: comparative aspects and future prospects. *Virology* 435, 14–28. doi: 10.1016/j.virol.2012.10.007

Brandler, S., Marianneau, P., Loth, P., Lacote, S., Combredet, C., Frenkiel, M. P., et al. (2012). Measles vaccine expressing the secreted form of West Nile virus envelope glycoprotein induces protective immunity in squirrel monkeys, a new model of West Nile virus infection. *J. Infect. Dis.* 206, 212–219. doi: 10.1093/infdis/jis328

Despres, P., Combredet, C., Frenkiel, M. P., Lorin, C., Brahic, M., and Tangy, F. (2005). Live measles vaccine expressing the secreted form of the West Nile virus envelope glycoprotein protects against West Nile virus encephalitis. *J. Infect. Dis.* 191, 207–214. doi: 10.1086/426824

Fujino, M., Yoshida, N., Kimura, K., Zhou, J., Motegi, Y., Komase, K., et al. (2007). Development of a new neutralization test for measles virus. *J. Virol. Methods* 142, 15–20. doi: 10.1016/j.jviromet.2007.01.001

Griffin, D. E. (2007). "Measles virus," in *Fields Virology*, eds D. M. Knipe, P. M. Howley, D. E. Griffin, R. A. Lamb, M. A. Martin, B. Roizman, and S. E. Straus, 5 Edn (Philadelphia: Lippincott Williams & Wilkins, a Wolters Kluwer Business), 1551–1585.

Hamaia, S., Li, C., and Allain, J. P. (2001). The dynamics of hepatitis C virus binding to platelets and 2 mononuclear cell lines. *Blood* 98, 2293–2300. doi: 10.1182/blood.V98.8.2293

Hashimoto, K., Ono, N., Tatsuo, H., Minagawa, H., Takeda, M., Takeuchi, K., et al. (2002). SLAM (CD150)-independent measles virus entry as revealed by recombinant virus expressing green fluorescent protein. *J. Virol.* 76, 6743–6749. doi: 10.1128/JVI.76.13.6743-6749.2002

Hummel, K. B., Lowe, L., Bellini, W. J., and Rota, P. A. (2006). Development of quantitative gene-specific real-time RT-PCR assays for the detection of measles virus in clinical specimens. *J. Virol. Methods* 132, 166–173. doi: 10.1016/j.jviromet.2005.10.006

Ito, R., Takahashi, T., Katano, I., and Ito, M. (2012). Current advances in humanized mouse models. *Cell. Mol. Immunol.* 9, 208–214. doi: 10.1038/cmi.2012.2

Jiang, Q., Zhang, L., Wang, R., Jeffrey, J., Washburn, M. L., Brouwer, D., et al. (2008). FoxP3+CD4+ regulatory T cells play an important role in acute HIV-1 infection in humanized Rag2−/−gammaC−/− mice in vivo. *Blood* 112, 2858–2868. doi: 10.1182/blood-2008-03-145946

Kato, S. I., Nagata, K., and Takeuchi, K. (2012). Cell tropism and pathogenesis of measles virus in monkeys. *Front. Microbiol.* 3:14. doi: 10.3389/fmicb.2012.00014

Kimberly, W. T., Zheng, J. B., Town, T., Flavell, R. A., and Selkoe, D. J. (2005). Physiological regulation of the beta-amyloid precursor protein signaling domain by c-Jun N-terminal kinase JNK3 during neuronal differentiation. *J. Neurosci.* 25, 5533–5543. doi: 10.1523/JNEUROSCI.4883-04.2005

Koga, R., Ohno, S., Ikegame, S., and Yanagi, Y. (2010). Measles virus-induced immunosuppression in SLAM knock-in mice. *J. Virol.* 84, 5360–5367. doi: 10.1128/JVI.02525-09

Lin, W. H., Kouyos, R. D., Adams, R. J., Grenfell, B. T., and Griffin, D. E. (2012). Prolonged persistence of measles virus RNA is characteristic of primary infection dynamics. *Proc. Natl. Acad. Sci. U.S.A.* 109, 14989–14994. doi: 10.1073/pnas.1211138109

Lorin, C., Mollet, L., Delebecque, F., Combredet, C., Hurtrel, B., Charneau, P., et al. (2004). A single injection of recombinant measles virus vaccines expressing human immunodeficiency virus (HIV) type 1 clade B envelope glycoproteins induces neutralizing antibodies and cellular immune responses to HIV. *J. Virol.* 78, 146–157. doi: 10.1128/JVI.78.1.146-157.2004

Ohno, S., Ono, N., Seki, F., Takeda, M., Kura, S., Tsuzuki, T., et al. (2007). Measles virus infection of SLAM (CD150) knockin mice reproduces tropism and immunosuppression in human infection. *J. Virol.* 81, 1650–1659. doi: 10.1128/JVI.02134-06

Reyes-del Valle, J., Hodge, G., Mcchesney, M. B., and Cattaneo, R. (2009). Protective anti-hepatitis B virus responses in rhesus monkeys primed with a vectored measles virus and boosted with a single dose of hepatitis B surface antigen. *J. Virol.* 83, 9013–9017. doi: 10.1128/JVI.00906-09

Sawada, A., Komase, K., and Nakayama, T. (2011). AIK-C measles vaccine expressing fusion protein of respiratory syncytial virus induces protective antibodies in cotton rats. *Vaccine* 29, 1481–1490. doi: 10.1016/j.vaccine.2010.12.028

Sellin, C. I., and Horvat, B. (2009). Current animal models: transgenic animal models for the study of measles pathogenesis. *Curr. Top. Microbiol. Immunol.* 330, 111–127. doi: 10.1007/978-3-540-70617-5_6

Singh, M., Cattaneo, R., and Billeter, M. A. (1999). A recombinant measles virus expressing hepatitis B virus surface antigen induces humoral immune responses in genetically modified mice. *J. Virol.* 73, 4823–4828.

Stebbings, R., Fevrier, M., Li, B., Lorin, C., Koutsoukos, M., Mee, E., et al. (2012). Immunogenicity of a recombinant measles-HIV-1 clade B candidate vaccine. *PLoS ONE* 7:e50397. doi: 10.1371/journal.pone.0050397

Sun, Z., Denton, P. W., Estes, J. D., Othieno, F. A., Wei, B. L., Wege, A. K., et al. (2007). Intrarectal transmission, systemic infection, and CD4+ T cell depletion in humanized mice infected with HIV-1. *J. Exp. Med.* 204, 705–714. doi: 10.1084/jem.20062411

Tatsuo, H., Ono, N., Tanaka, K., and Yanagi, Y. (2000). SLAM (CDw150) is a cellular receptor for measles virus. *Nature* 406, 893–897. doi: 10.1038/35022579

Terahara, K., Ishige, M., Ikeno, S., Mitsuki, Y. Y., Okada, S., Kobayashi, K., et al. (2013). Expansion of activated memory $CD4^+$ T cells affects infectivity of CCR5-tropic HIV-1 in humanized NOD/SCID/JAK3^{null} mice. *PLoS ONE* 8:e53495. doi: 10.1371/journal.pone.0053495

Traggiai, E., Chicha, L., Mazzucchelli, L., Bronz, L., Piffaretti, J. C., Lanzavecchia, A., et al. (2004). Development of a human adaptive immune system in cord blood cell-transplanted mice. *Science* 304, 104–107. doi: 10.1126/science.1093933

Wege, A. K., Melkus, M. W., Denton, P. W., Estes, J. D., and Garcia, J. V. (2008). Functional and phenotypic characterization of the humanized BLT mouse model. *Curr. Top. Microbiol. Immunol.* 324, 149–165. doi: 10.1007/978-3-540-75647-7_10

Conflict of Interest Statement: The authors declare that the research was conducted in the absence of any commercial or financial relationships that could be construed as a potential conflict of interest.

Received: 07 August 2013; accepted: 17 September 2013; published online: 11 October 2013.

Citation: Ikeno S, Suzuki M, Muhsen M, Ishige M, Kobayashi-Ishihara M, Ohno S, Takeda M, Nakayama T, Morikawa Y, Terahara K, Okada S, Takeyama H and Tsunetsugu-Yokota Y (2013) Sensitive detection of measles virus infection in the blood and tissues of humanized mouse by one-step quantitative RT-PCR. Front. Microbiol. 4:298. doi: 10.3389/fmicb.2013.00298

This article was submitted to Virology, a section of the journal Frontiers in Microbiology.